DAVIS, KLINTON P., Ph.D. Sol-Gel Synthesis and Band Gap Engineering of Zinc Oxide Nanostructures. (2021)
Directed by Dr. Hemali Rathnayake. 104 pp.

Zinc Oxide (ZnO) belongs to the (II-VI) wurtzite semiconductor that has found practical applications across multiple disciplines. One of its first main uses was in the application of ultraviolet protection (sunscreen) since it has a bandgap that absorbs in the UV. In more recent years, researchers have been manipulating ZnO properties, specifically its bandgap, to use it as an alternative for applications that require hazardous and toxic materials. This dissertation focuses on developing sol-gel based synthesis methods to tailor electronic properties of ZnO. The sol-gel methods developed in this dissertation provides understanding of how size, shape, and composition of ZnO can be controlled by nucleation growth followed by solvent-driven self-assembly processes. Through this modified sol-gel synthesis approach, the use of dopant materials can be introduced using mostly first row transition metals and showed morphology changes as well as mixed crystal structures, leading to changes in optical and electronic properties.

From the first project, the modified sol-gel synthesis made use of six organic solvents showed that solvent choice plays a role in the morphology of zinc oxide but also affects its electronic structure in terms of optical bandgap. The solvents act as a surfactant and through the promotion of Oriented Attachment allowing nanorods, nanospheres, and nanoslates to be formed. The optical bandgap showed that there was a wide range between the solvents but after annealing showed similar values of 3.37 eV showing that the solvents were on the surface of the nanostructures as a surfactant. TEM and X-ray diffraction showed all morphologies were highly crystalline except DMSO having a wide

peak at the [101] due to the grain size of the structure. Overall, DMF is the preferred solvent due to its bandgap being similar to the others, high crystallinity, and solubility in the system. This shows that solvent choice can play a crucial role for modifying morphology and optical bandgap of ZnO.

The modified sol-gel synthesis was further tested with the incorporation of dopants into the system at different concentrations. Choosing DMF as the solvent due to the results of Aim 1, six dopants were tested having similar ionic radii or valency. The dopants were incorporated with the dopant metal ions ranging from 1-5 % across multiply trials to dope the ZnO nanorods. Results showed that morphology was not maintained by all but two, which were Copper and Erbium. All others had either changed morphology or had mixed morphology showing incompatibility for maintaining ZnO nanorod formation. It was also observed that Copper at higher concentrations of dopant was able to produce hierarchical structures leading to the idea that solvent choice with a dopant precursor could lead to more exotic structures in the future. Optical bandgap measurements were made and while all gave a blue shift from the original ZnO nanorods spectra, all were within tenths of an eV leading to no immediate favorite. X-ray diffraction was done and showed that the largest peak shifts were from copper and erbium, both of which formed nanorods. All other dopants caused a shift but was either minimal or had added peaks in the system further showing that the multiple morphologies were separate from the ZnO crystal lattice. In short, using the modified sol-gel method in the presence of DMF show promise for certain dopant metals.

The final project took the modified sol-gel synthesis and furthered the process by incorporating it as a core-shell system. Taking ZnO nanorods made in DMF, they were suspended in different concentration solutions of cobalt(II)nitrate under heat. The use of SEM showed nanoparticle formation occurred on the surface of the ZnO nanorods. Verification of the particles was done with (S)TEM/EDS showing the lattice spacing and elemental composition to be cobalt oxide. Using X-ray photoelectron spectroscopy, the cobalt oxide was determined to be in the Co^{2+} state.

SOL-GEL SYNTHESIS AND BAND GAP ENGINEERING OF ZINC OXIDE NANOSTRUCTURES

by

Klinton P. Davis

A Dissertation Submitted to
the Faculty of The Graduate School at
The University of North Carolina at Greensboro
in Partial Fulfillment
of the Requirements for the Degree
Doctor of Philosophy

Greensboro
2021

Approved by

_____
Committee Chair

APPROVAL PAGE

This dissertation, written by KLINTON P. DAVIS, has been approved by the following committee of the Faculty of The Graduate School at The University of North Carolina at Greensboro.

Committee Chair Hemali Rathnayake

Committee Members Daniel J. Herr

Tetyana Ignatova

Jeffrey Alston

03/22/21
Date of Acceptance by Committee

03/22/21
Date of Final Oral Examination

TABLE OF CONTENTS

Page

LIST OF FIGURES

Page

CHAPTER I

INTRODUCTION

1.1 Zinc Oxide

Alternative materials are constantly being discovered for a multitude of applications to replace them with more efficient and cost-effective materials.[1] What is often overlooked is the need to look into materials that are not toxic and hazardous as well.[1] In the realm of semiconductors this holds especially true. While the materials currently used in industry are highly effective, and they do have some systems in place to recycle these materials safely, certain semiconductor industries lack this infrastructure. This, in turn, causes these materials to go to landfill and pollute the environment. The solar industry has only been around for a few decades and has made great strides to produce green energy. It is with a heavy heart to state that while the purpose of the product is ecofriendly, the process and the materials used are not. Here we discuss the use of zinc oxide as an alternative material to possibly replace even one aspect of these current devices.

Zinc oxide as a material has multiple benefits that allows it to be a potential candidate for a replacement material in the solar industry. First, it is incredibly safe to handle in bulk form. One of the first applications of zinc oxide was sunscreen and has been used in toothpaste. The next argument is abundance with zinc being the 24th most abundant element in the earths' crust with the annual production being around 11,900,000

tonnes along with zinc oxide being relatively cheap and easy to process. Most importantly though are its material properties. Its hexagonal crystal structure allows the material to be a piezoelectric material due to the asymmetrical geometry of the crystal. Both crystal variants, the other being cubic, are mostly transparent material as a thin film that has a high electron mobility and wide optical bandgap that borders the visible spectrum.

1.2 Zinc Oxide in Devices

From almost every piece of literature, it is stated that the hexagonal wurtzite structure with a 3.37 eV large bandgap and a 60 meV exciton radius of zinc oxide (ZnO) makes it a viable option for devices.[1–4] Whether it be for energy harvesting, biosensors, piezoelectric, to gas sensors, ZnO has a variety of applications.[3,5–10] Probably one of the most underutilized characteristics of ZnO is the ability to control its morphology. From the plain thin film to the nanorod, ZnO has probably as many shape varieties as gold. Depending on what synthetic scheme is used, the possibilities can be vast.[3]

Taking a certain amount of material of the same mass and cutting that mass into nanoscale units has drastic effects on its properties. One of the more prominent reasons why we care to change morphology is to study its electronic structure. By shrinking sizes down to the nanoscale, certain properties change such as bandgap or charge transfer mechanisms.[11] This is demonstrated by comparing thin films to its nanostructure form, where by increasing the surface area, the more a material is able to transfer electrons to an acceptor when dealing with photovoltaics. In fact, in a p-n system the effective length an electron can viably travel to another material is approximately 10 nm leading to the

statement of, for thick materials it is mostly wasted space. ZnO specifically has an electron travel distance of 1.8 nm.[1] When it comes to the nanoscale, the number one dominating factor everyone talks about is the increased surface area. By increasing this aspect of the system, you allow any material to interact much greater for whatever application it is being used. Therefore, controlling morphology and dimension become imperative when optimizing for electronics.

1.2.1 Wet Chemical Synthesis of ZnO

There is a push to make synthesis as green as possible restricting the scientist to basic solvents such as ethanol and water. While non-aqueous synthesis has been done it is not as accepted since some of these chemicals can be toxic to the environment and the scientist.[12,13] An argument can be made that solvent driven morphological studies have not progressed as far as other methods. Solvent driven synthesis can offer a pathway for more controllable morphologies for ZnO and possibly other systems as well. Taking advantage of how solvents are aprotic, protic, and non-polar can lead to alternative methods that could possibly be more desirable tailoring the nucleation and crystal growth to achieve size and shape-controlled metal oxide nanostructures. By taking advantage of specific features, namely polarity and steric hinderance of a solvent, there are definitely ways to control the formation and growth of ZnO nanostructures. For these reasons the choice has been made to pursue this study in hopes of finding easier methods for morphology control of ZnO-based nanomaterials.

1.2.2 Doping ZnO with Binary and Tertiary Metals

Doping has been proven to be an effective method for changing certain properties, specifically electrical properties. By creating defects in the lattice of any crystal, bonding orbitals dilate or contract depending on the dopant used.[14] This results in other properties, like bandgap, to be changed to an extent.[14] While doping is a common method for changing bandgap, a major component that is left out is how well morphology of the original system can be maintained. One type of system where doping does not affect morphology is when nanorods are grown on thin films. This is mainly due to the thin film having localized sections of crystal structure called grains where the growth orientation is orthogonal to the plane. These grains act as nucleation sites for the precursor material to bind along with the dopant metal to form nanorods. While the dimension of nanorods may change in thickness and/or in length, they are still aligned nanorods. For a sol-gel synthesis with no substrate acting as a scaffold, localized dopant metal may kinetically act faster than the zinc hydroxides form. This would leave a minimal amount of dopant hydroxides that would have a significant impact on the morphologies. This leads to deviations from the original synthesis and can yield undesirable results. One instance is ZnO being doped with iron in different concentrations turning zinc oxide nanorods into iron doped zinc oxide nanospears, which for biological applications would have disastrous consequences.[15]

1.2.3 ZnO Core/Shell Systems

The use of core/shell systems have the unique advantage of the starting material already being well defined and only needs post modification.[16] High controllability has

been achieved however the use of toxic solvents, capping agents, and precisely controlled environments make this method somewhat unappealing even though the method is well defined.[17] An example comes from (Schaak et al.) where there base particle is a copper sulfide (CuS) nanorod.[17] Through multiple cation exchanges they are able to obtained a highly mixed nanorod with eight different sections being of different elements and crystal structure. This method uses a one-pot synthesis method in inert atmospheric conditions ranging from 80 – 220℃ as well as chemicals such as benzyl ether, octadecene, and oleylamine. This dissertation will put forth effort into using aqueous means for post modification by only using concentration and temperature as parameters as there is little literature on a core/shell and cation exchange methods via green aqueous methods. This would push forth the sol-gel chemistry further into nanoparticle synthesis in terms of complexity and applications.

1.3 Current State of the Art

There are many variations for the synthesis of ZnO to tailor it to a specific application. As stated, anything from LEDs to chemical sensing.[6,18] In most applications, these methods prefer making either nanoparticles or nanorods using mostly aqueous experimental design. Some even take inspiration from plant extracts as a means to control size and morphology for a truly "green" synthesis.[19–24] Through spanning the space of variables, it is possible to get desired results with these chemicals. One thing that you will notice from literature is that while they are using water as the main solution, the precursor is typically an exotic nitrogen compounds like hexamethylenetetramine (HMTA) that facilitates growth.[25,26] Therefore, the goal of this project is to expand sol-gel synthesis

with the introduction of organic solvents to the sol phase. This will allow possible new structures to be synthesized and an alternate means of achieving known nanostructures. By developing this modified sol-gel method, it leads to how organic solvents would affect the morphology if divalent or trivalent cations were added as a dopant material to the sols.

Once again, doping has been used for a variety of applications. In the case of zinc oxide, most try to take advantage of its tetrahedral coordination bonding as a crystal for sensing applications.[27–29] The other is for its optical properties specifically solar cells or for catalytic properties.[29,30] In a more general sense, zinc oxide in terms of single element doping is not uncommon, with D. Lee et al. noting there have been 61 dopant elements that have been used in zinc oxide to modify its properties from over 500 papers.[29] By adding a dopant precursor and mixing it with our zinc sol in the presence of common organic solvents, the field can gain insight and further its understanding for modified sol-gel synthesis.

As this dissertation suggests, modification of zinc oxide using eco-friendly methods is one of the main topics. Another way modification can happen is the introduction of a shell material around our nanostructures making a core/shell system. A core/shell system can happen using one of two routes with the first being growth on the zinc oxide particle. For thin film applications of zinc oxide aligned nanorods, this process is well understood. Using atomic layer deposition, the nanorods can be uniformly coated with any appropriate metal that can closely match its crystalline structure.[31] For sol-gel systems, care must be taken to ensure that functional groups, surfactants, or pH balance are

compatible to give the greatest probability for this system to occur. In Yadzi et al. they make the choice of ammonia to change the pH to 10, under vigorous stirring at multiple temperatures.[32] Ammonia was chosen since it weakly binds to the Fe_3O_4 and as zinc acetate in ethanol is introduced, the zinc ion replaces the ammonia resulting it as a byproduct. This would more than likely not work if the base was potassium hydroxide sin the OH^- group is a stronger bond to the iron oxide particle. The second method would be ion exchange which is the replacement of atoms vs growing. Schaak et al. demonstrates this by using CuS of quantized dimensions and while maintaining size and shape, has a change of composition in eight regions.[17] As mentioned prior, this method has its drawback in that high temperatures are used in inert conditions with hazardous chemicals. Here, the goal is to eliminate the need for high pH or hazardous experimental setup by controlling parameters in aqueous conditions.

1.4 General Goals of Research

Overall dissertation hypothesis:

"Sol-gel based wet chemical synthesis methods followed by solvent driven self-assembly processes will provide a path to tailor properties of ZnO nanomaterials and its binary metal-doped structures."

Rationale:

While modification of ZnO to tailor its bandgap has been done, what has been done via physical processes, not much work has been demonstrated using wet-chemical synthesis methods, in particular, an aqueous method at low temperatures. Controllability of ZnO in terms of size and shape remain elusive, which holds especially true for

nanorods in particular. Nanoparticles are easily made via ball milling, capping with coordination compounds, and other high temperature methods.[17,25,33] However, nanorods of high uniformity specifically with nanorods using aqueous routes as well as the modification of them have not been reported. Hence, there is a need to explore possible alternatives for making ZnO nanorods in large scale via environmentally benign aqueous-based methods.

Addressing the overall hypothesis, this research proposes three specific aims:

Aim 1 - Developing a sol-gel based environmentally benign synthesis method to make size and shape controlled ZnO nanostructures.

Hypothesis – Polarity of the solvent will drive the nanocrystals (sols) self-assembly while the solvent acts as a surfactant, adsorbing onto the crystal facets with the highest surface energy.

Rationale: The synthesis of ZnO using the sol-gel process provides sols to self-assemble into different shapes and sizes, where crystal growth can either follow Ostwald Ripening mechanism or Oriented Attachement mechanism, or both. Also, sol-gel method is chosen due to the ease, affordability, and scalability to industrial applications. In typical shape controlled ZnO nanomaterials preparation, amine-based solvents are employed as a base and for the coordination of zinc ions to form structures. While these methods are great for control experiments, the main problem is short chain amines are hazardous. Therefore, the choice is made to use an alternate green route, while providing a path to control the dimensionality via self-assembly process.

Expected outcome:

Aim 1 will result in: A sol-gel based solvent polarity driven synthesis method to make ZnO nanostructures with different controlled morphologies, thus this method can be used to discover new morphologies of metal oxides from other binary and tertiary transition metals.

Aim 2 – Exploring a sol-gel based synthesis method to make bi/trimetallic oxide nanostructures by doping ZnO nanorods with di/trivalent metal precursors.

Hypothesis – Doping the wurtzite ZnO crystal structure with other binary and tertiary transition metal ions with the same size and valence may have an effect on the electronic properties of ZnO nanorods.

Rationale: By controlling the morphology through our solvent based synthesis method, fine tuning will result in particles that mean cation exchange conditions to further change the bandgap of the material.

Expected outcome:

Aim 2 will result in: (1) An understanding of how experimental design can affect the morphology of the same system. (2) Optimizing conditions so that dopants can integrate into the lattice without disruption of morphology.

Aim 3 – Developing Core/Shell method using aqueous solutions

Hypothesis – Making core/shell systems typically require harsh environments, however we should be able to manipulate an aqueous system via thermodynamics to achieve the same result.

Rationale: By choosing an appropriate candidate for the shell material, specifically one with the same oxidation state, this will allow favorable conditions. Then by manipulating saturation and temperature, the precursor should favor the zinc oxide as a nucleation site and grow uniformly on the surface.

Expected outcome:

Aim 3 will result in: (1) A relatively green and simple method to make core/shell systems using first row transition metals. (2) Extending this procedure to thin film applications via solar cells.

1.5 Dissertation Layout

This dissertation has been organized under six Chapters. The First chapter starts with an overview of zinc oxide and its relevance towards semiconductors. This will also go into detail as to why ZnO is an attractive material. For the second chapter, an in-depth background will be discussed covering all aspects on how to modify ZnO through multiple wet-chemical synthesis routes. Chapter III will discuss the approach and methods used and briefly discuss the reasoning behind them. The fourth chapter will give a full description of the materials used and the experimental setup used for each of the three aims. In the fifth chapter are the results and discussion of each of the three aims. The first aim being how solvent choice can affect the morphology of ZnO during growth as well as how it changes the bandgap of the system. The next project is to have zinc oxide as a core material and form a shell using the binary transition metal cobalt. The third aim will be how to incorporate other binary and ternary metals as a dopant material to ZnO in order to change the bandgap of the material. In Chapter VI, an overall

conclusion of the research will be described as well as possible future studies and recommendations.

1.6 References

(1) Klingshirn, C. F. ZnO: Material, Physics and Applications. *ChemPhysChem* **2007**, *8* (6), 782–803.

(2) Moezzi, A.; McDonagh, A. M.; Cortie, M. B. Zinc Oxide Particles: Synthesis, Properties and Applications. *Chem. Eng. J.* **2012**, *185–186*, 1–22.

(3) Wang, Z. L. Zinc Oxide Nanostructures: Growth, Properties and Applications. *J. Phys. Condens. Matter* **2004**, *16* (25), 829–858.

(4) Janotti, A.; Van De Walle, C. G. Fundamentals of Zinc Oxide as a Semiconductor. *Reports Prog. Phys.* **2009**, *72* (12).

(5) Panigrahi, S.; Sarkar, S.; Basak, D. Metal-Free Doping Process to Enhance the Conductivity of Zinc Oxide Nanorods Retaining the Transparency. *ACS Appl. Mater. Interfaces* **2012**, *4* (5), 2709–2716.

(6) Willander, M.; Nur, O.; Zhao, Q. X.; Yang, L. L.; Lorenz, M.; Cao, B. Q.; Žiga Pérez, J.; Czekalla, C.; Zimmermann, G.; Grundmann, M.; et al. Zinc Oxide Nanorod Based Photonic Devices: Recent Progress in Growth, Lightemitting Diodes and Lasers. *Nanotechnology* **2009**, *20* (33).

(7) Sato, K.; Katayama-Yoshida, H. Electronic Structure and Ferromagnetism of Transition-Metal-Impurity-Doped Zinc Oxide. *Phys. B Condens. Matter* **2001**, *308–310*, 904–907.

(8) Mondal, Kunal; Sharma, A. Recent Advances in Electrospun Metal-Oxide Nanofiber Based Interfaces for Electrochemical Biosensing. *RSC* **2016**, No. 6, 94595–94616.

(9) Kachynski, A. V.; Kuzmin, A. N.; Nyk, M.; Roy, I.; Prasad, P. N. Zinc Oxide Nanocrystals for Nonresonant Nonlinear Optical Microscopy in Biology and Medicine. *J. Phys. Chem. C* **2008**, *112* (29), 10721–10724.

(10) Wahab, H. A.; Salama, A. A.; El Saeid, A. A.; Willander, M.; Nur, O.; Battisha, I. K. Zinc Oxide Nano-Rods Based Glucose Biosensor Devices Fabrication. *Results Phys.* **2018**, *9*, 809–814.

(11) Van Embden, J.; Jasieniak, J.; Mulvaney, P. Mapping the Optical Properties of CdSe/CdS Heterostructure Nanocrystals: The Effects of Core Size and Shell Thickness. *J. Am. Chem. Soc.* **2009**, *131* (40), 14299–14309.

(12) Zhao, S.; Yan, W.; Shi, M.; Wang, Z.; Wang, J.; Wang, S. Improving Permeability and Antifouling Performance of Polyethersulfone Ultrafiltration Membrane by Incorporation of ZnO-DMF Dispersion Containing Nano-ZnO and Polyvinylpyrrolidone. *J. Memb. Sci.* **2015**, *478*, 105–116.

(13) Hu, Z.; Oskam, G.; Searson, P. C. Influence of Solvent on the Growth of ZnO Nanoparticles. *J. Colloid Interface Sci.* **2003**, *263* (2), 454–460.

(14) Özgür, Ü.; Alivov, Y. I.; Liu, C.; Teke, A.; Reshchikov, M. A.; Doğan, S.; Avrutin, V.; Cho, S. J.; Morkǫ, H. A Comprehensive Review of ZnO Materials and Devices. *J. Appl. Phys.* **2005**, *98* (4), 1–103.

(15) Lunin, A. V.; Sokolov, I. L.; Zelepukin, I. V.; Zubarev, I. V.; Yakovtseva, M. N.; Mochalova, E. N.; Rozenberg, J. M.; Nikitin, M. P.; Kolychev, E. L. Spindle-like MRI-Active Europium-Doped Iron Oxide Nanoparticles with Shape-Induced Cytotoxicity from Simple and Facile Ferrihydrite Crystallization Procedure. *RSC Adv.* **2020**, *10* (12), 7301–7312.

(16) Zhao, H.; Rosei, F. Colloidal Quantum Dots for Solar Technologies. *Chem* **2017**, *3* (2), 229–258.

(17) Steimle, B. C.; Fenton, J. L.; Schaak, R. E. Rational Construction of a Scalable Heterostructured Nanorod Megalibrary. *Science (80-.).* **2020**, *367* (6476), 418–424.

(18) Ansari, S. G.; Wahab, R.; Ansari, Z. A.; Kim, Y. S.; Khang, G.; Al-Hajry, A.; Shin, H. S. Effect of Nanostructure on the Urea Sensing Properties of Sol-Gel Synthesized ZnO. *Sensors Actuators, B Chem.* **2009**, *137* (2), 566–573.

(19) Selim, Y. A.; Azb, M. A.; Ragab, I.; H. M. Abd El-Azim, M. Green Synthesis of Zinc Oxide Nanoparticles Using Aqueous Extract of Deverra Tortuosa and Their Cytotoxic Activities. *Sci. Rep.* **2020**, *10* (1), 1–9.

(20) Thatoi, P.; Kerry, R. G.; Gouda, S.; Das, G.; Pramanik, K.; Thatoi, H.; Patra, J. K. Photo-Mediated Green Synthesis of Silver and Zinc Oxide Nanoparticles Using Aqueous Extracts of Two Mangrove Plant Species, Heritiera Fomes and Sonneratia Apetala and Investigation of Their Biomedical Applications. *J. Photochem. Photobiol. B Biol.* **2016**, *163*, 311–318.

(21) Govender, K.; Boyle, D. S.; Kenway, P. B.; O'Brien, P. Understanding the Factors That Govern the Deposition and Morphology of Thin Films of ZnO from Aqueous Solution? *J. Mater. Chem.* **2004**, *14* (16), 2575–2591.

(22) Ahsanulhaq, Q.; Umar, A.; Hahn, Y. B. Growth of Aligned ZnO Nanorods and Nanopencils on ZnO/Si in Aqueous Solution: Growth Mechanism and Structural and Optical Properties. *Nanotechnology* **2007**, *18* (11).

(23) Lepot, N.; Van Bael, M. K.; Van den Rul, H.; D'Haen, J.; Peeters, R.; Franco, D.; Mullens, J. Synthesis of ZnO Nanorods from Aqueous Solution. *Mater. Lett.* **2007**, *61* (13), 2624–2627.

(24) Spanhel, L.; Anderson, M. A. Semiconductor Clusters in the Sol-Gel Process: Quantized Aggregation, Gelation, and Crystal Growth in Concentrated ZnO Colloids. *J. Am. Chem. Soc.* **1991**, *113* (8), 2826–2833.

(25) Greene, L. E.; Yuhas, B. D.; Law, M.; Zitoun, D.; Yang, P. Solution-Grown Zinc Oxide Nanowires. *Inorg. Chem.* **2006**, *45* (19), 7535–7543.

(26) Strano, V.; Urso, R. G.; Scuderi, M.; Iwu, K. O.; Simone, F.; Ciliberto, E.; Spinella, C.; Mirabella, S. Double Role of HMTA in ZnO Nanorods Grown by Chemical Bath Deposition. *J. Phys. Chem. C* **2014**, *118* (48), 28189–28195.

(27) Han, C.; Duan, L.; Zhao, X.; Hu, Z.; Niu, Y.; Geng, W. Effect of Fe Doping on Structural and Optical Properties of ZnO Films and Nanorods. *J. Alloys Compd.* **2019**, *770*, 854–863.

(28) Poornaprakash, B.; Chalapathi, U.; Reddy, B. P.; Vattikuti, S. V. P.; Reddy, M. S. P.; Park, S. Magnetic Properties of Erbium Doped ZnO Nanoparticles.

(29) Yim, K.; Lee, J.; Lee, D.; Lee, M.; Cho, E.; Lee, H. S.; Nahm, H. H.; Han, S. Property Database for Single-Element Doping in ZnO Obtained by Automated First-Principles Calculations. *Sci. Rep.* **2017**, *7* (December 2016), 1–10.

(30) Mondal, A.; Giri, N.; Sarkar, S.; Majumdar, S.; Ray, R. Tuning the Photocatalytic Activity of ZnO by TM (TM = Fe, Co, Ni) Doping. *Mater. Sci. Semicond. Process.* **2019**, *91* (April 2018), 333–340.

(31) Law, M.; Greene, L. E.; Radenovic, A.; Kuykendall, T.; Liphardt, J.; Yang, P. ZnO-Al2O3 and ZnO-TiO2 Core-Shell Nanowire Dye-Sensitized Solar Cells. *J. Phys. Chem. B* **2006**, *110* (45), 22652–22663.

(32) Dehghani-Dashtabi, M.; Hekmatara, H.; Seyed-Yazdi, J. Synthesis and Improved Photoactivity of Magnetic Quaternary Nanocomposites Consisting of Fe3O4@ZnO Core@shell Nanoparticles Decorated on Graphene-Oxide Grafted Poly-Citric Acid. *Phys. B Condens. Matter* **2019**, *553* (October 2018), 11–17.

(33) Salah, N.; Habib, S. S.; Khan, Z. H.; Memic, A.; Azam, A.; Alarfaj, E.; Zahed, N.; Al-Hamedi, S. High-Energy Ball Milling Technique for ZnO Nanoparticles as Antibacterial Material. *Int. J. Nanomedicine* **2011**, *6*, 863–869.

CHAPTER II

BACKGROUND

2.1 Synthesis Methods to Prepare ZnO Nanostructures

The breadth of possibilities is endless for creating nanostructures. From top-down approaches reaching ordered features on the 7 nm scale, to bottom-up creating 1 nm CQDs.[1] All methods are viable and provide insight on strategies necessary to develop optimized systems. While there is a slew of different methods to synthesize and produce zinc oxide, the main way for the highest amount of variability and controllability would be through wet synthetic methods.

Bulk zinc oxide is of the II-VI *n*-type semiconductor group with a large, direct bandgap of 3.37 eV and exciton energy of 60 meV with gallium nitride being only 25 meV as a comparison.[2–5] Historically, ZnO was used as sunscreen since it effectively absorbs in the near ultraviolet range. This same material is still used in the rubber industry and plays a vital role in the vulcanization process.[4] Also, the large exciton energy means ZnO is not susceptible to trap site degradation that leads to a shorter lifetime for devices.[6]

Synthesizing ZnO nanostructures can result in a shift in the bandgap that is dependent on the size and morphology of the nanostructure. One of its more attractive features is the ability to synthesize many kinds of structures by just varying the technique or even the conditions of the same technique during the synthesis process. While a majority of the solar cells rely on a top-down approach, using a solvent-based bottom-up approach is a

viable method for zinc oxide. In Figure 2.1, the two main crystal orientations are shown to be cubic and wurtzite.[3] While the cubic formation has its uses, the hexagonal form is what makes it a notable contender for the electronics industry. Due to the asymmetric nature of a=b≠c, in hexagonal structures, ZnO as a piezoelectric is of high interest.[7,8] Also, with the hexagonal formation, it allows for better electrical conductivity pathways due to orientation and is almost exclusively the formation that is studied. For these reasons the rest of this discussion will focus solely the wurtzite crystal structure.

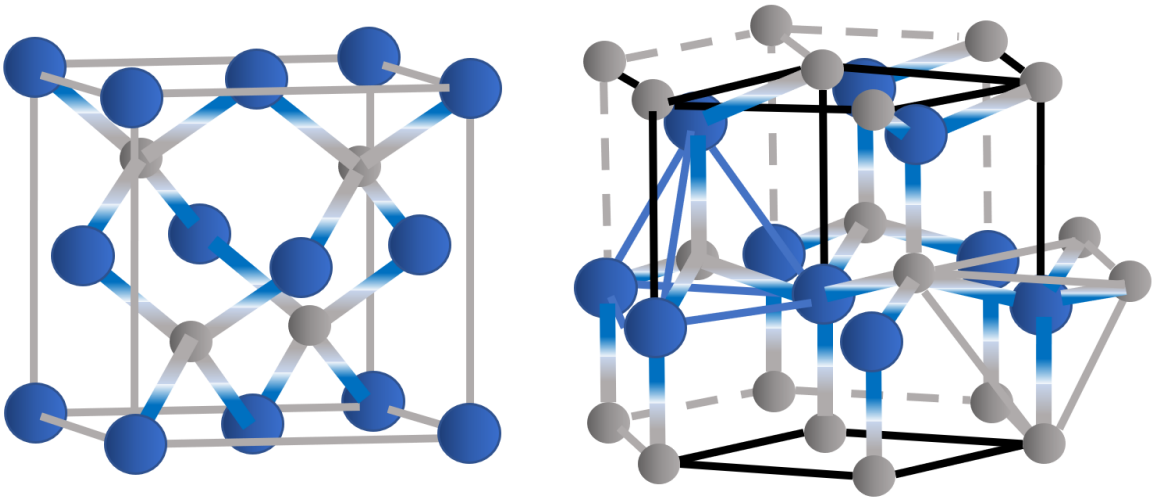

Zinc Blende Wurtzite

Figure 2.1. Crystal Variants of Zinc Oxide.

2.2 Sol-Gel Synthesis

The term sol-gel is the product of the first step being the breakdown of precursor material into a colloidal solution (sol) and then the combination of these sols into a network to create a larger system (gel) or gelation.[9] This category of synthesis is elementary by nature but has huge impacts for certain systems. One of the main things to

consider in these reactions is the amounts of starting precursor material as well as the volume in which it is dispersed into. On top of this, heat dependence can play a huge factor in terms of dimensional uniformity and even morphology. Even the rate at which you add precursor material can affect the system. With so many nuanced variables it is important to take into consideration what the goal of the synthesis should be as well as have some insight for what could or could not happen. An excellent example of sol-gel is the synthesis of silica nanoparticles.

The Stöber method is a specific example of the sol-gel process using tetraethoxysilane (TEOS) and water.[10] It is a two-step process in which we introduce TEOS into water and let the solution mix which allows hydrolysis to happen. This results in the formation of ethoxyethanols and with time and/or heat condenses into a Si-O matrix that can form gels or particles depending on the conditions. Condensation is simply the process that the reaction produces water or ethanol as an end product. Hydrolysis and condensation are very important aspects for the sol-gel process especially when it comes to metal oxides and their synthesis.

2.3 Metal Oxides

When working with metal oxides and their synthesis, it is often preferred to use their metal alkoxide forms since they react very well with water and the only by products are typically ethanol and/or water. As stated, when the metal alkoxide is introduced into water or ethanol, metal hydroxides form in the hydrolysis step. Then with time and heat, they grow into their desired structures with easy cleanup. For thin film applications, these

precursors can be in gas canisters and used for very precise control over thickness and even surface roughness. The big downside to metal alkoxides is that they can be unstable in ambient conditions and require inert and or moisture-free conditions in order to use them effectively. This is why we choose to look for alternative precursor materials in hopes of safely producing the same quality product.

Figure 2.2. Schematic Showing Typical Synthesis Pathway for Metal Oxides. Top: Alkyl Halide Elimination, Middle: Ether Elimination, Bottom: Condensation (Ester or Amide Elimination).

Within these synthetic reactions, it is possible to control morphology and dimensionality of the system. This can be achieved by addition of capping agents, ion concentration, pH, or even clever choice of precursor. In Figure 2.3, all morphologies shown are the result of one type of synthesis with clever choice in precursor and initial conditions through vapor liquid solid (VLS) deposition.[3] While this method can be versatile, issues arise when energy consumption is put under observation. This method involves very high sustained temperatures for significant periods of time. More so, with the amount of variation a system can generate to yield a vast amount of results, troubleshooting can be quite extensive at times. For these reasons wet synthetic methods are preferred and almost exclusively discussed.

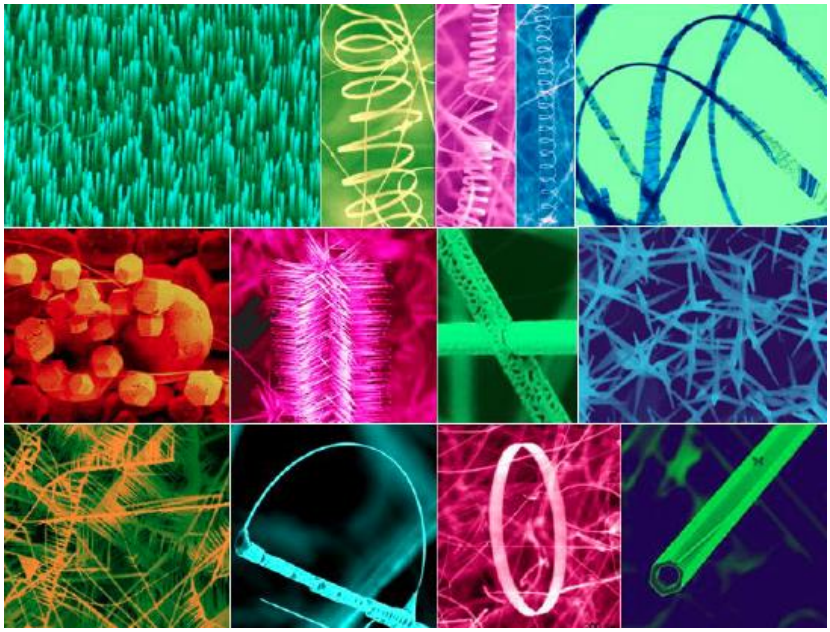

Figure 2.3. Different ZnO Morphologies. Wang, Z. L. Zinc Oxide Nanostructures: Growth, Properties and Applications. *J. Phys. Condens. Matter* **2004**, *16* (25).

2.4 Nanoparticle Growth Process and Mechanisms

The LaMer mechanism is an old but relevant primary theory of how nanoparticles form in wet synthesis conditions.[11] This mechanism is a three-stage process shown in Figure 2.4. The first stage is the precursor material is already broken down into its fundamental form, a monomer, the reaction starts and the monomers get concentrated together to form clusters, which is necessary for particle growth, or nucleation. Second stage is after the initial gathering of monomer clusters, there is thermodynamic relaxation thus drops below the nucleation threshold. Stage three is once the monomers are below the nucleation threshold and aggregation occurs to form particles by the addition of monomers to the surface of the growing particle. This particle growth is known as

Ostwald Ripening.[12] Ostwald Ripening typically gives unfavorable size dispersion of particles. While there can be additions that could be made to the primary theory, this is the most accepted.

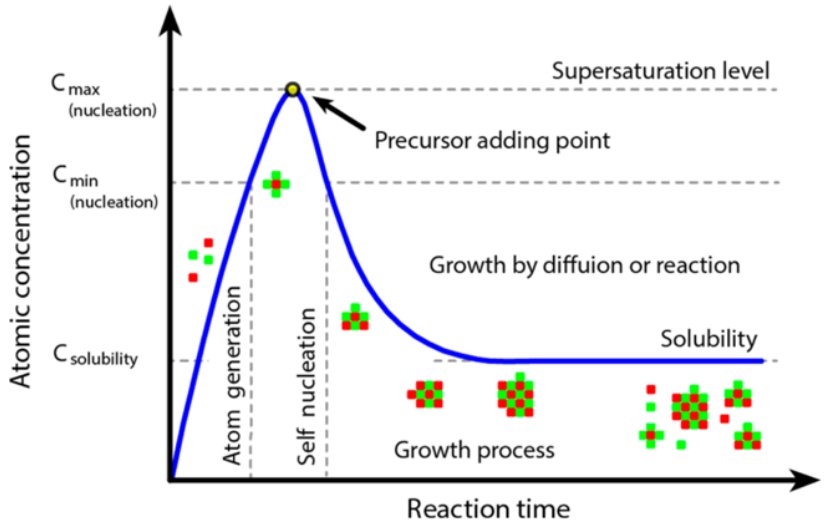

Figure 2.4. LaMer Mechanism. *Cryst. Growth Des.* 2017, 17, 2, 794–799.

Ostwald ripening is the process of a nucleation site for crystal growth, but due to poly crystallinity or non-homogeneity of the solution, crystals being fused, twinned, and leads to size inequality in the system. For nanoparticle systems, Ostwald ripening can be thought of as the "gel" portion of sol-gel synthesis. The main difference is that it is not an amorphous gel but discrete particles for metal oxide systems. As stated, Ostwald ripening is the main cause for vast dispersions in size. This is due to the fact that during stage two and conditions set, there are a certain number of nuclei within the closed system and have a maximum size equal to the amount of precursor divided by the number of nucleation sites. "While the number of nuclei formed can undoubtedly be altered through the choice

of reaction conditions, systematic, predictable control of nucleation is extremely difficult."[13]

A mechanism that has the ability to control the Ostwald Ripening process is the used of Oriented Attachment. As ripening occurs in the system experimental parameters can be chosen to ensure certain morphologies from the crystal growth. By using organic solvents in the system, they will interact with the sols of the ZnO and bind to crystal facets that are preferred or have the highest surface energy to the crystal.[14] From this, crystal growth is inhibited along these facets and promoting growth in another direction.[15] By categorization of solvent, trends and tendencies can be deduced that could lead into nanostructures that have better aspect ratios or even new shapes that have advantageous design. This feature of using organic solvents is primarily due to the difference in polarity as well as surface adhesion during crystal growth.[16,17] While other parameters like pH control and ion concentration do affect the morphology to a certain degree, Oriented Attachment if more selective and controllable.

2.5 Green Synthesis for Metal Oxides

As mentioned prior, the ability to control the number of nuclei or rather, control the overall particle dimensions for the final product is quite challenging. Add to the equation that we are also trying to control morphology and the problem is even more difficult. In order to alleviate this problem, the focus will be what precursor and what wet synthetic system can be used to control these effects. While precursor will be saved for discussion later, the solution to the solution is using mixed conditions with a variety of

solvents. As mentioned, most literature prefers conditions such as methanol, ethanol, and/or water. This is mainly due to those solutions being environmentally friendly and waste is non-hazardous. However, this mindset is limiting as well as simply disregarding other solvents. Bear in mind that the LaMer mechanism is a three-stage process where the first two stage have more to do with the chemistry of the solution rather than particle formation. From that, we can formulate the idea of different solvents may promote and/or restrict growth in terms of size and shape. By using aprotic, protic, or non-polar solvents, the ability to control these two factors should be possible. Based on the dipole of the solvent and other factors, the solvents will bind to specific crystal facets promoting or inhibiting growth, promoting rather than self-assembly driven Orientated Attachment mechanism for the formation of 1D anisotropic morphologies. For reference, a non-polar aliphatic chain like octadecene will typically form spherical particles because the solvent has no bias with how it interacts with the beginning nuclei.[18]

In order to fix the problem of using difficult precursor materials, attempts have been made to use alternatives. With the choice of precursor material changed, the next question becomes how to control these systems effectively? It's for this reason we choose metal precursors that come in the form of salts like chlorides, sulfates, nitrates, and so on. Furthermore, the type of precursor could have a tendency to form other morphologies in certain systems.[19] This is where we can take advantage of how nucleation is achieved and use solvents to drive the morphology into a certain configuration. The main problem with these precursors is the by product is usually not so easy to clean on top of which the

ligand present can have a large effect on the overall synthesis in general. So not only does the chemist need to consider the starting material but also the by-product leftover (side reactions). For this reason, most syntheses choose reactions whose side products can be easily washed with water.

Of course, there needs to be a way to manipulate the morphology to get the desired result. This in turn leads us into what parameters could be changed to reach the overall effect. One answer is pH for the system, by making conditions more basic or acidic, there can be preferred crystal growth along a certain axis. This has been shown in ZnO that if pH is below 9.0 then the morphology will be sheets, 9.0 and above they tend to form rods.[19,20] Likewise, choice of solvent can equally play a major role in determining crystal orientation and growth of nanomaterials. However, there are still major factors to consider when doing these kinds of syntheses with one being uniformity.

2.6 Doping and Core-Shell Synthesis

Synthesis methods vary in terms of how to dope zinc oxide. The method used is to dilute amounts of dopant precursor during the sol process so that it incorporates in the lattice evenly. Typical dopant levels can range from 5% to one to one hundred million in the case of silicon semiconductor wafers. Common elements for doping specifically to shift the bandgap of ZnO are typically magnesium and cadmium. Figure 2.5 shows how the conduction and valence bands would behave if dopants were introduced into the ZnO system. Cadmium would represent a bandgap reduction of 3.0 eV while magnesium would expand the bandgap to 4.0 eV.

When doping is considered, it is important to understand how dopant materials will fit into a system. One thing to consider is the valency of the dopant while another is its ionic radius. As one might suspect, magnesium is used as a dopant because its ionic radius closely resembles zinc allowing it to fit comfortably within the lattice. What causes the bandgap to shift for this case is the fact that magnesium uses its p orbital to have electrons flow vs zinc and its d orbital. On the other end, cadmium is directly below zinc on the periodic table and would have similar properties. The notable difference is it has a larger ionic radius causing a strain to the wurtzite crystal, this causes orbitals to shift and thus result in a bandgap shift.

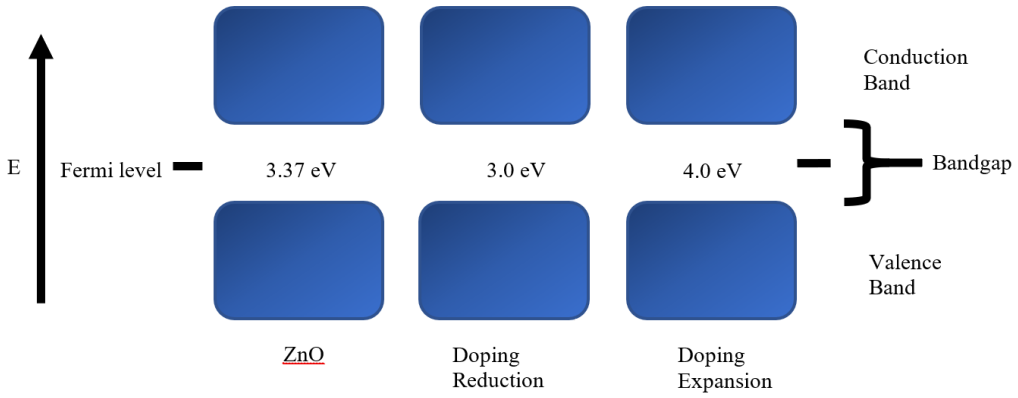

Figure 2.5. Bandgap Shift Diagram.

An important discussion is why doping is considered in the first place. In essence, a foreign element adds a certain strain on the crystal lattice. From this strain, orbital bonds shrink and/or stretch causing the valence and conduction bands to either expand or contract. This effectively changes the bandgap of the system and this is why doping is a preferred method when changing electronic properties of materials. In Figure 2.6 is the

wurtzite crystal and a substitute atom of the same oxidation state of +2 replacing the zinc. Another thing to note is optical properties can also be altered such as photoluminescence by doping the system.

Note that the dopant will only be replacing the cation in the system, zinc. Doping in regards to the oxygen remains somewhat elusive and quite difficult. This is mainly due to oxygen acting as a "deep donor" in the system making it challenging. The phrase deep donor comes from how the oxygen bandgap is positioned from valence to conduction band calculations indicating that oxygen is further away from the conduction band in terms of energy.[21] Meaning it is unwilling to share electrons and is highly bound to the system.

Something that is rarely brought up is that while doping may seem like an effortless process, many things can and will go wrong in the synthesis. If you are trying to dope using different oxidation state materials, consideration must be taken to understand which reaction will dominate and react faster. If the dopant material is consumed before growth of the main system happens then there is no chance of doping.

Other things to note are that if other metals are introduced then there is a probability that different morphologies can be produced aside from the original configuration. For first row transition metals in particular, they are known for their color chemistry due to their strong affinity to coordination of solvents. Due to the strong affinity, care must be taken as to how to remove these coordination bonds and incorporate the dopant into the zinc oxide growth system. This can be avoided based on

the kind of reaction and for hydrolysis and condensation, the mechanism is heat. Therefore, with thorough stirring and constant monitoring of the temperature to make sure the condensation step does not occur, confidence in the system being doped can happen. A guaranteed way to do this would be to chill precursor and solution while mixing so there are no localized condensation reaction spots within the system. Another way around this problem that might have more appeal is the use of post-synthesis methods, specifically Core-Shell systems.

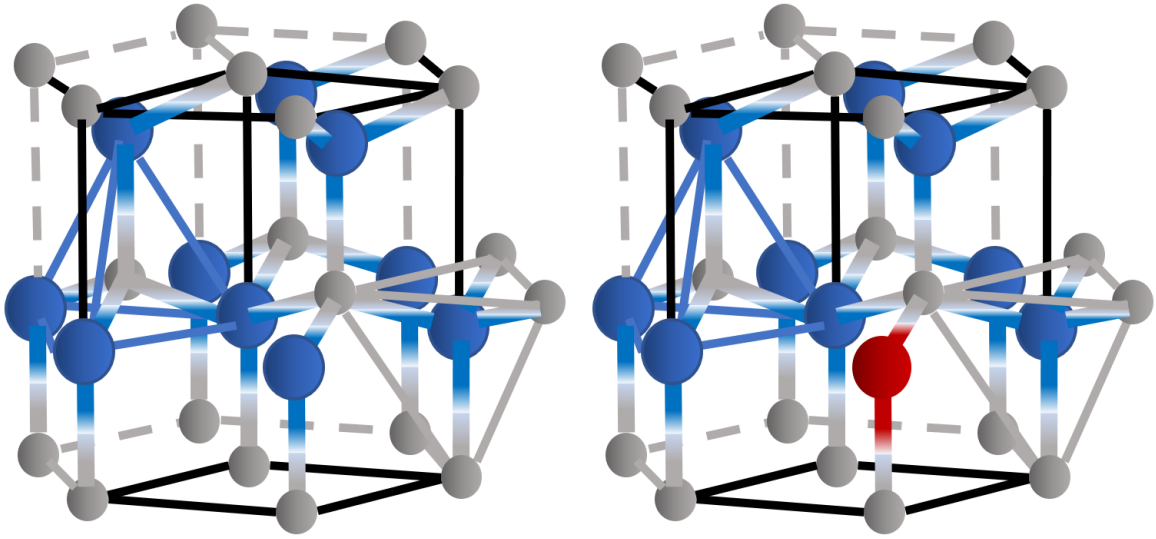

Figure 2.6. Doping Diagram with an Atom of the Same Valency.

Core-Shell (CS) systems offer a unique instance where adding a shell to a system causes a change in bandgap.[22–25] These systems are highly tunable and generally have narrow bandgap regions. What makes this method more exciting is the fact that multilayering is a possible allowing for great control over bandgap tunability. In Figure 2.7 there is a multitude of ways to adjust a CS nanoparticles. The one thing to note is in

Figure 2.6 (e, f, g) and how there are two layers involved. The first two can be simply labeled core-shell-shell (CSS) and it is important to remember that not all materials are compatible for CS nanoparticle systems whether it be the crystal structure or poor lattice matchup. Therefore, an intermediary layer can be used to passivate the two materials to achieve the desired effect. The final figure is a quantum dot/quantum well (QDQW) has been adapted to have precise shell thickness. An important thing to remember about all these CS nanoparticles is they are typically under 10 nm in at least one dimension. Furthermore, some materials have a bandgap that is dependent upon surface plasmon resonance and the interaction of the two materials at the interfacial layer is what causes a shift in bandgap.[26–28] Even the number of monolayers of the shell can determine the bandgap depending on the material.

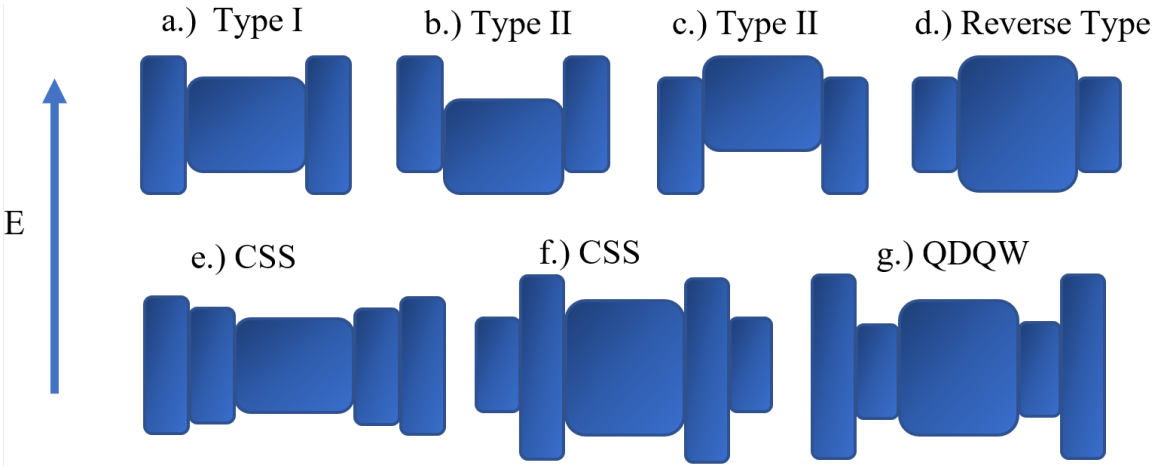

Figure2.7. Core-Shell Bandgap Diagram.

In terms of how these CS systems are attained, the hot injection method is one of the most common ways to produce metal chalcogenide and bimetallic CS systems.[29] This

is typically done as a one pot synthesis due to the reaction being sensitive to moisture and air. Figure 2.8 shows the overall scheme is to make your particles that will act as the core and wash away any undesirable by products (ideally there is none) by flowing inert gas in the solution or forming a precipitate that can be extracted easily. The next step would be the addition of the second precursor material at some high temperature that will react with the surface of the already synthesized particle making a shell. This method has proven quite capable and flexible for a variety of metal Core-Shell systems but is quite involved and can use toxic materials. As the for the astute observer that might notice, these systems would typically have no oxygen present in the reaction because most reactions typically get ruined by it. However, inspiration can be taken from this method and be developed for the purposes of this dissertation. For this reason, we look to cation exchange.

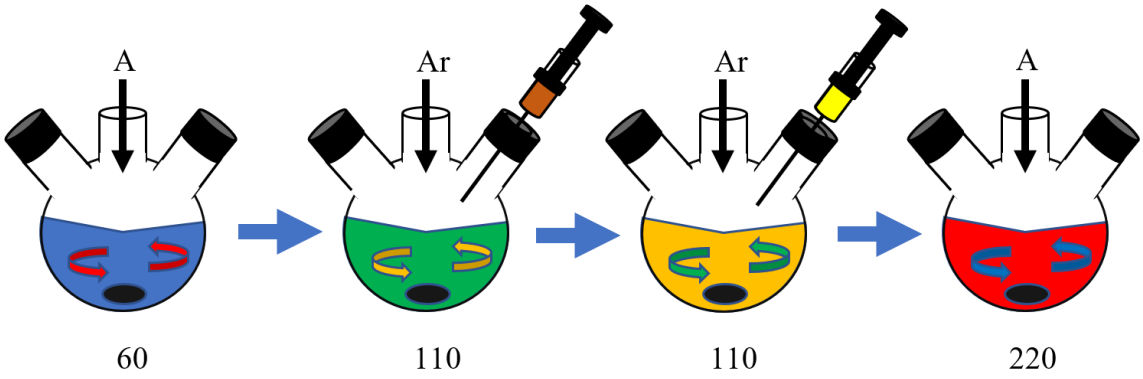

Figure 2.8. Typical Hot Injection Method Procedure.

Cation exchange is the process of either kinetically or thermodynamically driven substitution of one atom for another.[30] In general, substitution of atoms happens only at a

maximum of 10 nm. This leads to the statement that a full cation exchange process can only happen with a particle that is 20 nm in at least one dimension. This technique utilizes different solubilities of metal ions, such that the more soluble metal will get removed and be replaced with the metal dopant. In this case, outer zinc atoms will be replaced with the dopant metal precursor by varying concentration of the solution in different solvents after the ZnO nanorods are already made. This is advantageous since the synthesis process is only the addition of a step at the end versus changes or modifications during the known synthesis. While this only affects only a couple outer layers of ZnO, the exciton energy is large enough so that the ZnO core will still be part of the n-p transitions with a device as well as the shell of ZnO:M

One example of this method is CdSe to Ag_2Se as seen in Figure 2.9.[30] This also uses the hot injection method but the mechanism is different as stated earlier. The paper clearly demonstrates that cation exchange not only replaces the atoms in the particle but depending on the initial size, it can change shape as well. When the initial size is within range of the reaction zone width, the nanorod CdSe wurtzite crystal goes to a nanoparticle as it changes to Ag_2Se.

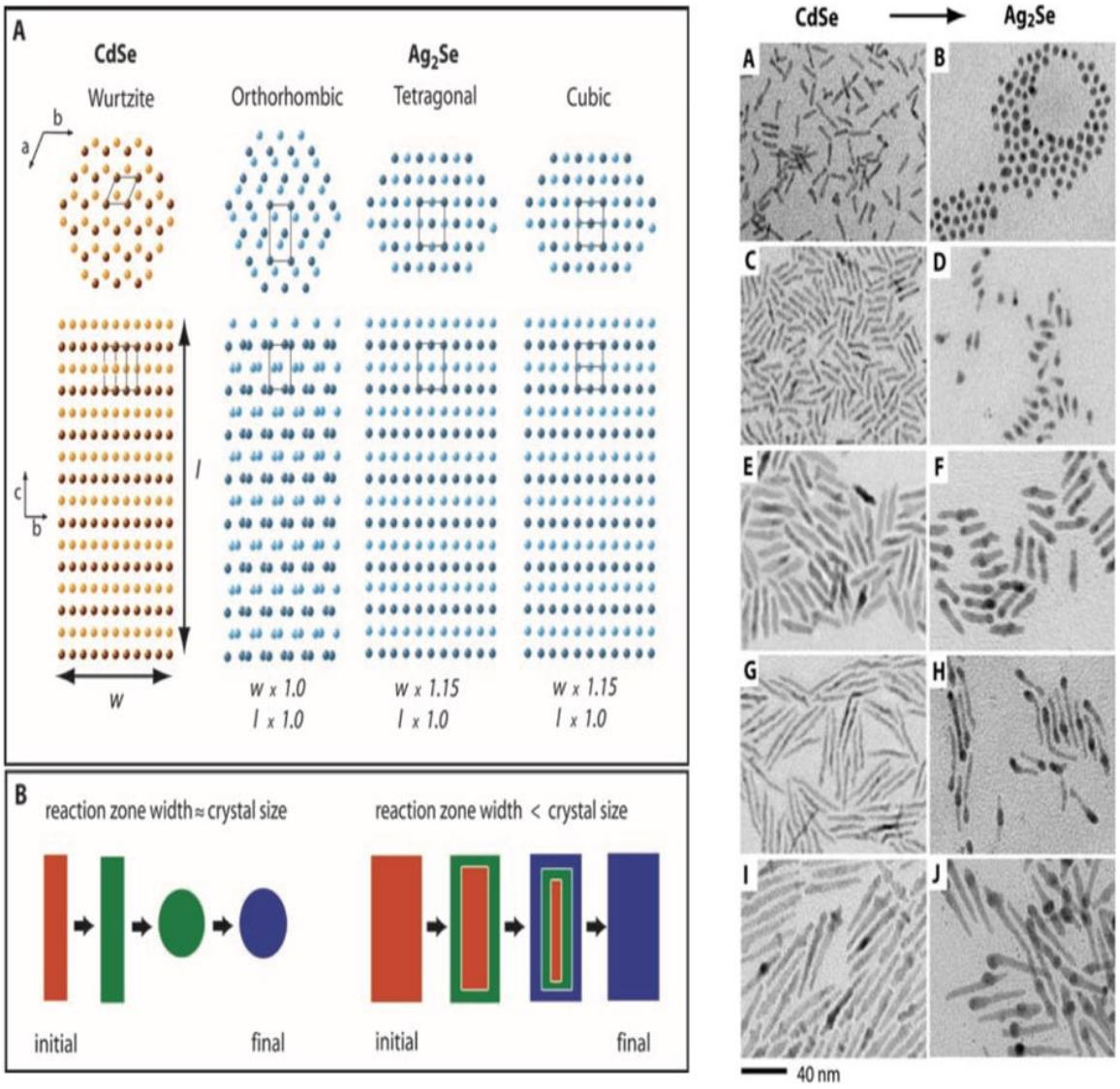

Figure 2.9. Cation Exchange Reactions in Ionic Nanocrystals. Dong Hee Son, *et al.* *Science* **306**, 1009 (2004).

2.7 References

(1) Xu, X.; Ray, R.; Gu, Y.; Ploehn, H. J.; Gearheart, L.; Raker, K.; Scrivens, W. A. Electrophoretic Analysis and Purification of Fluorescent Single-Walled Carbon Nanotube Fragments. *J. Am. Chem. Soc.* **2004**, *126* (40), 12736–12737.

(2) Klingshirn, C. F. ZnO: Material, Physics and Applications. *ChemPhysChem* **2007**, *8* (6), 782–803.

(3) Wang, Z. L. Zinc Oxide Nanostructures: Growth, Properties and Applications. *J. Phys. Condens. Matter* **2004**, *16* (25).

(4) Moezzi, A.; McDonagh, A. M.; Cortie, M. B. Zinc Oxide Particles: Synthesis, Properties and Applications. *Chem. Eng. J.* **2012**, *185–186*, 1–22.

(5) Willander, M.; Nur, O.; Zhao, Q. X.; Yang, L. L.; Lorenz, M.; Cao, B. Q.; Žiga Pérez, J.; Czekalla, C.; Zimmermann, G.; Grundmann, M.; et al. Zinc Oxide Nanorod Based Photonic Devices: Recent Progress in Growth, Lightemitting Diodes and Lasers. *Nanotechnology* **2009**, *20* (33).

(6) Luo, J.; Wang, Y.; Zhang, Q. Progress in Perovskite Solar Cells Based on ZnO Nanostructures. *Sol. Energy* **2018**, *163* (January), 289–306.

(7) Zhao, M. H.; Wang, Z. L.; Mao, S. X. Piezoelectric Characterization Individual Zinc Oxide Nanobelt Probed by Piezoresponse Force Microscope. *Nano Lett.* **2004**, *4* (4), 587–590.

(8) Agrawal, R.; Espinosa, H. D. Giant Piezoelectric Size Effects in Zinc Oxide and Gallium Nitride Nanowires. A First Principles Investigation. *Nano Lett.* **2011**, *11* (2), 786–790.

(9) Hench, L. L.; West, J. K. The Sol-Gel Process. *Chem. Rev.* **1990**, *90* (1), 33–72.

(10) Green, D. L.; Lin, J. S.; Lam, Y. F.; Hu, M. Z. C.; Schaefer, D. W.; Harris, M. T. Size, Volume Fraction, and Nucleation of Stober Silica Nanoparticles. *J. Colloid Interface Sci.* **2003**, *266* (2), 346–358.

(11) Lamer, V. K.; Dinegar, R. H. Theory, Production and Mechanism of Formation of Monodispersed Hydrosols. *J. Am. Chem. Soc.* **1950**, *72* (11), 4847–4854.

(12) Yec, C. C.; Zeng, H. C. Synthesis of Complex Nanomaterials via Ostwald Ripening. *J. Mater. Chem. A* **2014**, *2* (14), 4843–4851.

(13) Vreeland, E. C.; Watt, J.; Schober, G. B.; Hance, B. G.; Austin, M. J.; Price, A. D.; Fellows, B. D.; Monson, T. C.; Hudak, N. S.; Maldonado-Camargo, L.; et al. Enhanced Nanoparticle Size Control by Extending LaMer's Mechanism. *Chem. Mater.* **2015**, *27* (17), 6059–6066.

(14) Zhang, Jing; Huang, Feng; Lin, Z. Progress of Nanocrystalline Growth Kinetics Based on Oriented Attachment. *Nanoscale* **2010**, *2*, 18–34.

(15) Jun, Y. W.; Casula, M. F.; Sim, J. H.; Kim, S. Y.; Cheon, J.; Alivisatos, A. P. Surfactant-Assisted Elimination of a High Energy Facet as a Means of Controlling the Shapes of TiO2 Nanocrystals. *J. Am. Chem. Soc.* **2003**, *125* (51), 15981–15985.

(16) Peng, X.; Manna, L.; Yang, W.; Wickham, J.; Scher, E.; Kadavanich, A.; Alivisatos, A. P. Shape Control of CdSe Nanocrystals. *Nature* **2000**, *404* (6773), 59–61.

(17) Nguyen, T. D.; Dinh, C. T.; Do, T. O. Monodisperse Samarium and Cerium Orthovanadate Nanocrystals and Metal Oxidation States on the Nanocrystal Surface. *Langmuir* **2009**, *25* (18), 11142–11148.

(18) Steimle, B. C.; Fenton, J. L.; Schaak, R. E. Rational Construction of a Scalable Heterostructured Nanorod Megalibrary. *Science (80-.).* **2020**, *367* (6476), 418–424.

(19) Greene, L. E.; Yuhas, B. D.; Law, M.; Zitoun, D.; Yang, P. Solution-Grown Zinc Oxide Nanowires. *Inorg. Chem.* **2006**, *45* (19), 7535–7543.

(20) Alenezi, M. R.; Alshammari, A. S.; Jayawardena, K. D. G. I.; Beliatis, M. J.; Henley, S. J.; Silva, S. R. P. Role of the Exposed Polar Facets in the Performance of Thermally and UV Activated ZnO Nanostructured Gas Sensors. *J. Phys. Chem. C* **2013**, *117* (34), 17850–17858.

(21) Maharjan, N.; Mulmi, D. Das; Nakarmi, M. L. Optical Transitions in Lysozyme Mediated Zinc Oxide Nanoparticles Probed by Deep UV Photoluminescence. *Optik (Stuttg).* **2020**, *202* (July 2019), 163622.

(22) Li, Z.; Wanjala, B.; Cernigliaro, G.; Nawrocki, D.; Gu, Z. Synthesis of Zn2SiO4@ZnO Core-Shell Nanoparticles and the Effect of Shell Thickness on Band-Gap Transition. *Mater. Chem. Phys.* **2020**, *240* (November 2018), 122144.

(23) Yang, S.; Prendergast, D.; Neaton, J. B. Strain-Induced Band Gap Modification in Coherent Core-Shell Nanostructures. *Nano Lett.* **2010**, *10* (8), 3156–3162.

(24) Khanchandani, S.; Kundu, S.; Patra, A.; Ganguli, A. K. Band Gap Tuning of ZnO/In2S3 Core-Shell Nanorod Arrays for Enhanced Visible-Light-Driven Photocatalysis. *J. Phys. Chem. C* **2013**, *117* (11), 5558–5567.

(25) Song, J.; Ma, C.; Zhang, W.; Li, X.; Zhang, W.; Wu, R.; Cheng, X.; Ali, A.; Yang, M.; Zhu, L.; et al. Bandgap and Structure Engineering via Cation Exchange: From Binary Ag2S to Ternary AgInS2, Quaternary AgZnInS Alloy and AgZnInS/ZnS Core-Shell Fluorescent Nanocrystals for Bioimaging. *ACS Appl. Mater. Interfaces* **2016**, *8* (37), 24826–24836.

(26) Aziz, S. B.; Abdulwahid, R. T.; Rsaul, H. A.; Ahmed, H. M. In Situ Synthesis of CuS Nanoparticle with a Distinguishable SPR Peak in NIR Region. *J. Mater. Sci. Mater. Electron.* **2016**, *27* (5), 4163–4171.

(27) Xie, Y.; Chen, W.; Bertoni, G.; Kriegel, I.; Xiong, M.; Li, N.; Prato, M.; Riedinger, A.; Sathya, A.; Manna, L. Tuning and Locking the Localized Surface Plasmon Resonances of CuS (Covellite) Nanocrystals by an Amorphous CuPdxS Shell. *Chem. Mater.* **2017**, *29* (4), 1716–1723.

(28) Zhang, C.; Chen, B. Q.; Li, Z. Y.; Xia, Y.; Chen, Y. G. Surface Plasmon Resonance in Bimetallic Core-Shell Nanoparticles. *J. Phys. Chem. C* **2015**, *119* (29), 16836–16845.

(29) Ghosh Chaudhuri, R.; Paria, S. Core-Shell Nanoparticles: Classes, Properties, Synthesis Mechanisms, Characterization, and Applications. *Chem. Rev.* **2012**, *112* (4), 2373–2433.

(30) Dong, H. S.; Hughes, S. M.; Yin, Y.; Alivisatos, A. P. Cation Exchange Reactions in Ionic Nanocrystals. *Science (80-.).* **2004**, *306* (5698), 1009–1012.

CHAPTER III

APPROACH AND METHODS

Chapter III describes the three aims encompassing the ZnO system for modification. Dividing this chapter into two sections, the first will be the synthesis methods developed to make ZnO nanostructures and its bimetallic oxide nanostructures. Also, the choice of precursor material will be discussed in depth as to why these are appropriate choices. The other section will describe the characterization that will be used for each aim.

3.1 Methodology

3.1.1 Modified Synthesis of ZnO Nanostructures

When creating a synthetic scheme especially when dealing with nanostructures, it is of the utmost importance to understand all the variables involve in the system. In this modified sol-gel method, consideration must be taken for type of precursor (both zinc and oxygen source), the ratio between the precursors, the volume in which the reaction takes place, and other measurable parameters. This research has not been optimized in terms of yield or waste product as it is to find alternate pathways to find new morphologies, better doping strategies, and possible aqueous core/shell systems to improve bandgap and morphology control for better devices.

3.1.1.1 Discussion of Synthetic Pathway

The sol-gel method is a common way to make zinc oxide sols and typically cast onto substrates for growth of nanorods.[1–4] It is common practice to use water or ethanol for these sols since they are green and easily accessible. Here in this modified sol-gel method, we take this known reaction and add multiple solvents to the system varying in aprotic, protic, and non-polar to find correlations in how it affects the formation of ZnO and its morphology in solution. The solvents used were toluene, m-xylene, acetonitrile, dimethylformamide (DMF), dimethylsulfoxide (DMSO), and hydroquinone (HQ). The use of these solvents by taking advantage of van der waals interactions should facility oriented growth of the same crystal structure.[5–9] These chemicals were chosen on the basis that these are "common" solvents in a general chemistry lab and therefore easily accessible. Figure 3.1 gives a general schematic of how the synthesis will be done. The general set up will be having 0.21 g of $ZnCl_2$ and 0.40 g of NaOH dissolved in 30 mL of the solvent along with 5 mL of DI water. It is left to stir until the solution becomes clear. Heat is then applied and still stirring for 24 hours to form the nanostructures. The wash process was decanting the solvent afterwards and sonicating the product DI water in a falcon tube along with centrifugation afterwards for three cycles.

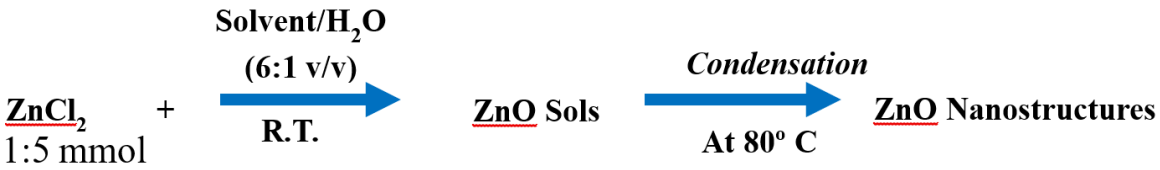

Figure 3.1. Reaction Scheme for Modified Sol-Gel Method.

Once the morphology, crystallinity, and uniformity are explored for each solvent, modification of the ZnO system will be done by using an alternate route to create core/shell will be explored for ZnO to see if aqueous methods are viable. Typically, the insertion and exchange of atoms in a system have a high energetic cost and therefore requires either high heat or pressure systems.[10,11] Solution based chemistry can be performed using chemicals such as benzyl ether, oleylamine, tri-actyl phosphine, and octadecene that results in core/shell systems.[12–15] The shell material precursor will be cobalt(II)nitrate and was chosen for its oxidation state which makes it more advantageous since it matches zinc's valence, size, and properties. Another reason is that other cobalt precursors like chlorides and acetates are also soluble in water, cobalt nitrate has the lowest melting point which could further aid if concentrations must be higher than the solubility of cobalt(II)nitrate. By changing concentrations in relation to the precursor material and heating, the cobalt precursor should bind to the outer layers where zinc oxide acts as a nucleation site to form CoO. Varying the concentrations should inherently change the kinetics of the solution in such a way that it will be energetically favorable for zinc to be replaced with cobalt in an aqueous system.[15,16] Figure 3.2 depicts the synthesis scheme. While doping with cobalt has been done, to date there has not been a good representation of ZnO with a cobalt shell.[17–20] This method builds on the synthesis of Aim 1 since the starting product is already made and the only modification is dispersing the ZnO NRs in a concentrated metal precursor solution and let it heat for a period of time.

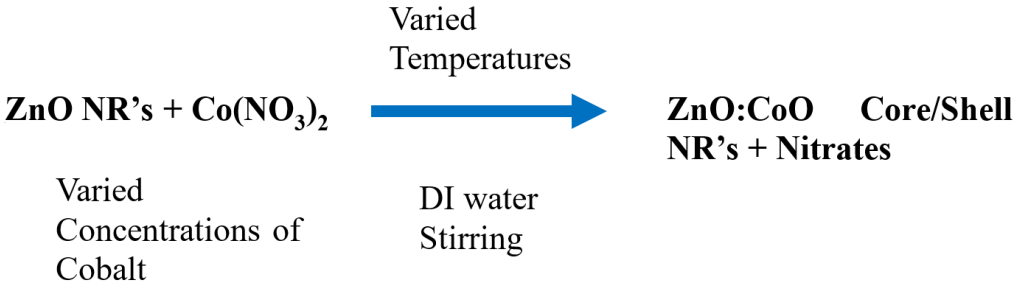

Figure 3.2. ZnO Core/Shell Diagram.

Afterwards, a comparison is made to synthesize and is incorporate cationic doping. The doping process involves mostly first row transition metals and multiple synthetic pathways are being explored. Doping is not difficult but doping to maintain morphology and uniformity of the nanostructure proves troublesome and great care must be taken in order to preserve these structures.[21–24] This is all to change the bandgap of the system. Figure 3.3 is a representative scheme of how this will be done. The procedure is essentially the same except the dopant precursor is added with the others.

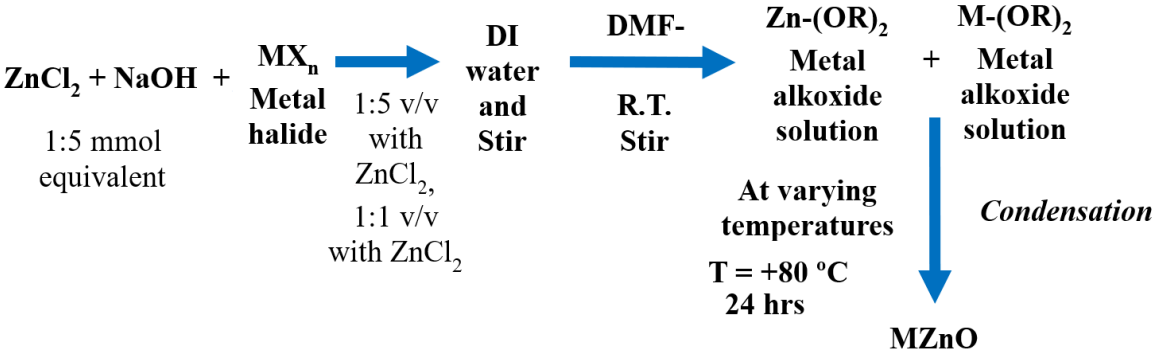

Figure 3.3. Doping Schematic of the System.

3.1.2 Research Goals

a.) Aim 1 - Developing a sol-gel -based environmentally benign synthesis method to make size and shape controlled ZnO nanostructures.

Hypothesis – Polarity of the solvent will drive the nanocrystals (sols) self-assembly while the solvent acts as a surfactant, adsorbing onto the crystal facets with the highest surface energy.

3.1.2.1 Method to Selection of Solvents and the Zinc Precursor

Solvents can interact with the growth process through a variety of means whether it is the dipole associated with the solvent, the shape of the molecule, or even side reactions from the precursor material. However, the most probable cause for the solvent giving ZnO determination in morphology would be to the solvent binding to the crystal facets when ZnO is in the sol stage. Therefore, the choice of precursor that make up the monomers in the reaction are highly important.

One of the main reasons ZnO was chosen was the fact that Zn only exists in a +2 state and therefore there is no concern of how solvents might drive different stoichiometric ratios for zinc oxide. Also, certain zinc precursors happen to be a fairly cheap in comparison to other transition metals and roughly 10^5 tons of zinc oxide are produced per year.[25] As far as the material used as the zinc precursor, the choice was zinc chloride ($ZnCl_2$) due to the byproduct being some form of salt. Also, while the goal is to make different nanostructures, ideally nanorods will be made for further modification. Metal Chlorides tend to form rods in certain conditions.[26] Because the byproduct is salt,

this makes cleaning the product fairly strait forward as only water will be needed for the wash process. As for the oxygen source, sodium hydroxide pellets (NaOH) will be used as the nucleophile to donate the OH group for the hydrolysis step. The choice of solvents that are being investigated, in the writers' opinion, are common solvents that are accessible to any lab. Predicting what morphologies would be difficult but due to the conditions being ran, rods and plates are to be expected.

To complete Aim 1, the research will follow (three) tasks.

Task 1: Sol-gel synthesis methods for ZnO.

Finding the optimal synthetic scheme for morphology and bandgap.

Characterization: UV-Vis**,** SEM

Task 2: Explore morphology and crystallinity of the ZnO Nanostructures.

Characterization: TEM, XRD

Task 3: Investigate electrical conductivities of ZnO Nanostructures.

Characterization: two probe I-V test system.

b.) Aim 2 – Exploring a sol-gel-based synthesis method to make bimetallic oxide nanostructures by doping ZnO nanorods with binary transition metal precursors.

Hypothesis – Doping the wurtzite ZnO crystal structure with another binary transition metal ion with same size and valence may have an effect on the electronic properties of ZnO nanorods.

3.1.2.2 Dopant Metal Precursor Selection for ZnO

Building on the modified sol-gel method, it is natural to explore the possibility of dopants to the system and well they behave. As mentioned prior, investigation of transition metals will be used for the dopant, specifically first row transition metals. First row transition metals offer great potential as they are similar in ionic radius to zinc.

The overall goal is to find a dopant with a certain synthetic scheme and maintain the original nanostructure made for ZnO. This proves to be quite the challenge for multiple reasons. First there is no guarantee that a specific pathway will work. Second, if the dopant material is released from its coordination with the solvent, there is the possibility that the dopant material will react faster, giving different morphologies of just the dopant material. And finally, there is no promises that the doped ZnO will have its original structure with the incorporation of the dopant.

To complete Aim 2, the research will follow (three) tasks.

Task 1: Doping ZnO.

Looking for shifts in optical bandgap.

Characterization: UV-Vis

Task 2: Explore morphology and crystallinity of the ZnO.

Characterization: SEM, TEM, XRD

Task 3: Investigate electrical and device plausibility.

Characterization: two probe I-V test system.

c) Aim 3 – Developing Core-Shell structure of ZnO:CoO bimetallic oxide structures via sol-gel synthesis.

Hypothesis – The stepwise sol-gel synthesis at low temperature will drive the self-assembly to form core-shell architectures.

3.1.2.3 Sol-gel synthesis Method for Core/Shell System

With exploration of doping the ZnO system with an optimal solvent and checking bandgap, crystallinity, and morphology, it would now be interesting to see if post modification of ZnO can be achieved. Granted this has been done, however there has not been a truly aqueous method to make ZnO into a core/shell system. For this reason, exploration into post modification will be done with cobalt(II)nitrate at different concentrations and temperatures.

To complete Aim 3, the research will follow (three) tasks.

Task 1: Making Cobalt Shell on ZnO as the core

Characterization: (S)TEM, EDS, SAED

Task 2: Exploring the chemical state of the cobalt shell.

Characterization: XPS

Task 3: Investigate electrical and device plausibility.

Characterization: two probe I-V test system.

3.2 Characterization

3.2.1 Bandgap

The method for measuring bandgap can be broken down into optical bandgap and electrical bandgap measurements. For the optical bandgap, using UV-Visible spectrophotometer will be the preferred method. Bandgap was calculated using Eq. 1 where h is Planck's constant, c is the speed of light, and λ is the wavelength.

$$E = \frac{h\,c}{\lambda} \qquad \text{(Eq. 1)}$$

3.2.1.1 Sample Preparation

Sample preparation for optical bandgap measurements were subjugated to standard testing beforehand to ensure consistency. ZnO solutions were diluted with IPA to be clear solutions and sonicated before measurements were made. All measurements were done in with a quartz cuvette and triplicate to ensure aggregation or light degradation occurred after an initial measurement was performed.

3.2.2 Morphology and Crystallinity

Morphology analysis were performed using a transmission electron microscope (Zeiss Libra 120 TEM) and a scanning electron microscope (Zeiss Auriga FIBFESEM). Crystallinity was investigated using selected area electron diffraction (SAED) along with an Oxford X-ray diffraction (XRD) using a copper source.

3.2.2.1 Sample Preparation

Sample preparation for SEM was performed through dilution of solution drop casted on a cleaved silicon wafer. Samples were washed with water multiple times and dispersed in IPA for uniform dispersion across the surface of the silicon. This same dispersion was used for TEM as well. XRD was performed using dry powder and adhering the powder to a fiberglass dipped in oil.

3.2.3 Electrical Properties

3.2.3.1 Sample Preparation

Because are dispersing particles, a drop cast method in water and will be used multiple times on the same substrate to get an appropriate thickness. This is so there will be no possibility of a short circuit when the probes connect to the surface. A glass substrate will be used so that there is no confusion in resistances of the substrate versus the material. Afterwards, a drying oven will be used to evaporate the water so that the conductivity measurements are just the ZnO system.

3.2.4 Chemical State Analysis

X-ray photoelectron spectroscopy (XPS) has been performed on the ZnO system. By investigating zinc, oxygen, and other metal precursor species, identification of oxidation state and mechanism can be achieved.

3.2.4.1 Sample Preparation

As with the electrical analysis, samples will be drop cast using water but on a silicon substrate. The ZnO system will have sufficient thickness so that oxide peaks from

the silicon do not appear. The silicon will be cleaved and wiped with IPA and sonicated in DI water to remove silicon remnants from the surface before the solution is drop cast.

3.3 References

(1) Xu, C. X.; Wei, A.; Sun, X. W.; Dong, Z. L. Aligned ZnO Nanorods Synthesized by a Simple Hydrothermal Reaction. *J. Phys. D. Appl. Phys.* **2006**, *39* (8), 1690–1693.

(2) Baruah, S.; Dutta, J. Effect of Seeded Substrates on Hydrothermally Grown ZnO Nanorods. *J. Sol-Gel Sci. Technol.* **2009**, *50* (3), 456–464.

(3) Tay, C. B.; Chua, S. J.; Loh, K. P. Investigation of Morphology and Photoluminescence of Hydrothermally Grown ZnO Nanorods on Substrates Pre-Coated with ZnO Nanoparticles. *J. Cryst. Growth* **2009**, *311* (5), 1278–1284.

(4) Kim, K. H.; Utashiro, K.; Abe, Y.; Kawamura, M. Structural Properties of Zinc Oxide Nanorods Grown on Al-Doped Zinc Oxide Seed Layer and Their Applications in Dye-Sensitized Solar Cells. *Materials (Basel).* **2014**, *7* (4), 2522–2533.

(5) Zhang, Jing; Huang, Feng; Lin, Z. Progress of Nanocrystalline Growth Kinetics Based on Oriented Attachment. *Nanoscale* **2010**, *2*, 18–34.

(6) Bodnarchuk, M. I.; Kovalenko, M. V.; Heiss, W.; Talapin, D. V. Energetic and Entropic Contributions to Self-Assembly of Binary Nanocrystal Superlattices: Temperature as the Structure-Directing Factor. *J. Am. Chem. Soc.* **2010**, *132* (34), 11967–11977.

(7) Smith, D. K.; Goodfellow, B.; Smilgies, D. M.; Korgel, B. A. Self-Assembled Simple Hexagonal AB2 Binary Nanocrystal Superlattices: SEM, GISAXS, and Defects. *J. Am. Chem. Soc.* **2009**, *131* (9), 3281–3290.

(8) Bian, K.; Wang, Z.; Hanrath, T. Comparing the Structural Stability of Pbs Nanocrystals Assembled in Fcc and Bcc Superlattice Allotropes. *J. Am. Chem. Soc.* **2012**, *134* (26), 10787–10790.

(9) Shevchenko, E. V.; Talapin, D. V.; Kotov, N. A.; O'Brien, S.; Murray, C. B. Structural Diversity in Binary Nanoparticle Superlattices. *Nature* **2006**, *439* (7072), 55–59.

(10) Schaak, R. E.; Mallouk, T. E. Perovskites by Design: A Toolbox of Solid-State Reactions. *Chem. Mater.* **2002**, *14* (4), 1455–1471.

(11) Feng, S.; Xu, R. New Materials in Hydrothermal Synthesis. *Acc. Chem. Res.* **2001**, *34* (3), 239–247.

(12) Steimle, B. C.; Fagan, A. M.; Butterfield, A. G.; Lord, R. W.; McCormick, C. R.; Di Domizio, G. A.; Schaak, R. E. Experimental Insights into Partial Cation Exchange Reactions for Synthesizing Heterostructured Metal Sulfide Nanocrystals. *Chem. Mater.* **2020**, *32* (13), 5461–5482.

(13) Casavola, M.; Van Huis, M. A.; Bals, S.; Lambert, K.; Hens, Z.; Vanmaekelbergh, D. Anisotropic Cation Exchange in PbSe/CdSe Core/Shell Nanocrystals of Different Geometry. *Chem. Mater.* **2012**, *24* (2), 294–302.

(14) Zhong, X.; Xie, R.; Zhang, Y.; Basché, T.; Knoll, W. High-Quality Violet- To Red-Emitting ZnSe/CdSe Core/Shell Nanocrystals. *Chem. Mater.* **2005**, *17* (16), 4038–4042.

(15) Rivest, J. B.; Jain, P. K. Cation Exchange on the Nanoscale: An Emerging Technique for New Material Synthesis, Device Fabrication, and Chemical Sensing. *Chem. Soc. Rev.* **2013**, *42* (1), 89–96.

(16) Luther, J. M.; Zheng, H.; Sadtler, B.; Alivisatos, A. P. Synthesis of PbS Nanorods and Other Ionic Nanocrystals of Complex Morphology by Sequential Cation Exchange Reactions. *J. Am. Chem. Soc.* **2009**, *131* (46), 16851–16857.

(17) Manthina, V.; Agrios, A. G. Facile Synthesis of Zn1−xCoxO/ZnO Core/Shell Nanostructures and Their Application to Dye-Sensitized Solar Cells. *Superlattices Microstruct.* **2017**, *104*, 374–381.

(18) Davis, M.; Gümeci, C.; Black, B.; Korzeniewski, C.; Hope-Weeks, L. Tailoring Cobalt Doped Zinc Oxide Nanocrystals with High Capacitance Activity: Factors Affecting Structure and Surface Morphology. *RSC Adv.* **2012**, *2* (5), 2061–2066.

(19) Dhruvashi; Shishodia, P. K. Effect of Cobalt Doping on ZnO Thin Films Deposited by Sol-Gel Method. *Thin Solid Films* **2016**, *612*, 55–60.

(20) AlTurki, A. M. Low-Temperature Synthesis of Core/Shell of Co3O4@ZnO Nanoparticle Characterization and Dielectric Properties. *J. Nanostructure Chem.* **2018**, *8* (2), 153–158.

(21) Chunxia, L.; Cuimiao, Z.; Zhiyao, H.; Lili, W.; Zewei, Q.; Hongzhou, L.; Jun, L. β-NaYF4 and β-NaYF4:Eu3+ Microstructures: Morphology Control and Tunable Luminescence Properties. *J. Phys. Chem. C* **2009**, *113* (6), 2332–2339.

(22) Xu, Z.; Kang, X.; Li, C.; Hou, Z.; Zhang, C.; Yang, D.; Li, G.; Lin, J. Ln3+ (Ln = Eu, Dy, Sm, and Er) Ion-Doped YVO4 Nano/Microcrystals with Multiform Morphologies: Hydrothermal Synthesis, Growing Mechanism, and Luminescent Properties. *Inorg. Chem.* **2010**, *49* (14), 6706–6715.

(23) Mao, C.; Yang, X.; Zhao, L. Simultaneous Morphology Control and Upconversion Fluorescence Enhancement of NaYF4: Yb,Er Crystals through Alkali Ions Doping. *Chem. Eng. J.* **2013**, *229*, 429–435.

(24) Kumar, Y.; Sahai, A.; Olive-Méndez, S. F.; Goswami, N.; Agarwal, V. Morphological Transformations in Cobalt Doped Zinc Oxide Nanostructures: Effect of Doping Concentration. *Ceram. Int.* **2016**, *42* (4), 5184–5194.

(25) Klingshirn, C. F. ZnO: Material, Physics and Applications. *ChemPhysChem* **2007**, *8* (6), 782–803.

(26) Greene, L. E.; Yuhas, B. D.; Law, M.; Zitoun, D.; Yang, P. Solution-Grown Zinc Oxide Nanowires. *Inorg. Chem.* **2006**, *45* (19), 7535–7543.

CHAPTER IV

EXPERIMENTAL SECTION

4.1 Sol-gel Synthesis of ZnO Nanostructures

4.1.1 Materials

Sodium hydroxide (98% purity), and zinc chloride (97% purity), were obtained from Aldrich Chemicals. Anhydrous dimethyl formamide, anhydrous dimethyl sulfoxide, meta-xylene, acetonitrile, hydroquinone, and toluene were used as received without any purification otherwise specified.

4.1.2 Characterization

Morphology analysis was done using a scanning electron microscope (Zeiss Auriga FIB/FESEM) and a transmission electron microscope (Zeiss Libra 120 TEM). Crystalline studies were performed using the TEM and an Agilent technologies Gemini X-ray Diffractometer using a copper source. Elemental Analysis we conducted using elemental dispersion spectroscopy (Bruker and Oxford EDS) and X-ray photoelectron spectrometry (Escalab Xi+ Thermos Scientific XPS). Optical properties were explored using a UV-Vis spectrometer (Varian Cary 6000i). Electrical properties were done using a Keithley source meter controlled by Photo Emission TEC. INC (PET) I–V test system.

4.1.3 Synthesis Procedure

ZnO Nanostructures were synthesis by wet chemical synthesis via aqueous based solvent system. $ZnCl_2$ was maintained at molar ratio to NaOH of 1:5 mmol. The metal

precursor measured out to 0.21 g and was first dissolved in the organic solvent equating to 30 mL and a solution of NaOH of 0.4g in 5 mL of DI water was added. The mixed solution was at room temperature and stirred for 15 minutes before raising the temperature to 80℃ in a sand bath. After another 60 minutes of stirring the stir bar was removed from the round bottom flask and maintained at 80℃ for 24 hrs. Note that the solution was at 80℃ and not the hot plate. A white solid was formed with a typical yield of 110 mg. The product was collected and washed through vortex, sonication, and centrifuged three times before any measurements were made.

4.2 Synthesis of ZnO Nanostructures with Binary Metal Ion Doping

4.2.1 Materials

Sodium hydroxide (98% purity), and zinc chloride (97% purity), zinc acetate, copper(II)acetate, iron(II)chloride, cobalt(II)chloride, magnesium(II)chloride, chromium(III)chloride, erbium(III)trifluoroacetate, and DMF

4.2.2 Characterization

Morphology analysis was done using a scanning electron microscope (Zeiss Auriga FIB/FESEM). Optical bandgap was explored using a UV-Vis spectrometer (Varian Cary 6000i). Crystalline studies were done on an Agilent technologies Gemini X-ray Diffractometer.

4.2.3 Synthesis Procedure

For the materials used with each other for the reaction, if the dopant metal was a chloride then zinc chloride was used and likewise zinc acetate if it was a metal acetate.

This was to prevent side reactions and keep the side products the same. Zinc chloride/ acetate and maintained at molar ratio to NaOH of 1:5 mmol. The metal precursor measured out to 0.21 g for zinc chloride and 0.26 g for zinc acetate. In the same 100 mL round-bottom flask, each dopant material was measured out to be in weight ratios of (0.1, 0.2, 0.3, 0.5, 1):1 mmol to the zinc chloride or zinc acetate. Finally, the sodium hydroxide was measured out to 0.4 g and placed in the same round bottom as the metal precursors. Then 5 mL of deionized water was added and stirred for 15 minutes to achieve homogeneity. Once stirring completed, 30 mL of dimethylformamide was then added dropwise into the solution while stirring at room temperature. After the addition of DMF, the round-bottom was place in an oil bath and heated to 105ºC for 24 hours with stirring.

Once the reaction is done, let the solution cool down to room temperature. Use a centrifuge at 10 krpm for 10 minutes and decant the solution from the product. Disperse the product in water by vortex and sonication. When the product is entirely removed from the wall of the falcon tube via sonication, sonicate for 5 minutes. This wash step should be done 3 times to ensure no salt is left in the system for future measurements. After the wash process is done, the product is frozen in liquid nitrogen to freeze excess water and placed in a freeze dryer for 24 hours.

4.3 Sol-gel Synthesis of ZnO Core-Shell Nanostructures

4.3.1 Materials

Sodium hydroxide (98% purity), and zinc chloride (97% purity), Cobalt(II)Nitrate (98%), and Deionized Water.

4.3.2 Characterization

Morphology analysis was done using a scanning electron microscope (Zeiss Auriga FIB/FESEM) and (Scanning) transmission electron microscope (JEM 2100 Plus 200kV ((S)TEM). Crystalline studies were performed using the TEM and an Agilent technologies Gemini using a copper source. Elemental Analysis we conducted using elemental dispersion spectroscopy (Oxford EDS) and X-ray photoelectron spectrometry (Escalab Xi+ Thermos Scientific XPS).

4.3.3 Synthesis Procedures

All synthesis starts with clean glassware. Using the same round bottom flask for the entire process, concentrated hydrochloric acid was used to remove any metal contaminates followed by DI water sonication. Once dry, a base bath mixture of IPA and potassium hydroxide was poured in the round bottom and sonicated to remove any organics left on the glass. Once sonicated again with DI water and dried, a second wash was done with concentrated hydrochloric acid with sonication to remove any metal salts that were produced as a result of the base bath. Multiple sonication with DI water is used to ensure the glass was chlorine free and the surface was layered with hydroxide groups. Rigorous cleaning is necessary to ensure the glassware in its entirety has the same surface chemistry to remove any variability in size and shell thickness of the ZnO NRs.

The synthesis of the ZnO NR were made by sol-gel synthesis. Zinc chloride was measured at 0.21 grams and dispersed in 30 mL in dimethylformamide which was then sonicated to break up the precursor. Sodium hydroxide was measured at 0.40 grams,

dispersed in 5 mL of deionized water and sonicated to break down the pellets. Each solution was then stirred for 10 minutes to guarantee homogeneity in each solution. The zinc chloride solution was put on ice so that when adding the sodium hydroxide solution, the heat from the initial reaction would not prematurely start the sol gel process. The sodium hydroxide solution was then added dropwise into the zinc chloride solution while stirring. As a note, flocculation will happen throughout this slow drip procedure. Have the solution stir until flocculation is not visible before adding the next drop. Ideally, you will be left with a translucent solution. Place the solution in a chilled sonication bath ≤ 10ºC (ideally 5ºC) for 5 minutes to break up any aggregation that accidentally happened. Afterwards stir for 15 minutes to let solution get to approximately room temperature, the solution should turn white by then. Place the round bottom on a hot plate that stirs and has a ceramic holder to ensure heat dispersion is uniform through your glass as well as cover it in aluminum foil to prevent any unnecessary cooling from the vents in the hood. Make sure to cap your round bottom. Once on, set the hot plate so that your solution is at 80ºC and hold for 24 hours while stirring.

Once done, let the solution cool down to room temperature. Use a centrifuge at 10 krpm for 10 minutes and decant the solution from the product. Disperse the product in water by vortex and sonication. When the product is entirely removed from the wall of the falcon tube via sonication, sonicate for 5 minutes. This wash step should be done 3 times to ensure no salt is left in the system for future measurements. After the wash process is done, the product is frozen in liquid nitrogen to freeze excess water and placed

in a freeze dryer for 24 hours. It is then annealed for two hours at 300ºC to set the crystal structure.

The core/shell synthesis will involve the same setup. A batch of pre-made ZnO nanorods of 0.05 g is first mixed in 15 mL of deionized water by sonication in the round bottom and then stirred for 15 minutes. Separately, cobalt nitrate was mixed in 15 mL of deionized water via sonication until the precursor completely dissolved into solution and then 15 minutes of stirring. Cobalt Nitrate was measured to amounts that were weight to weight of ZnO in ratios of 1:x, where x is an integer up to 10. After both mixtures reach 15 minutes of stirring, the cobalt nitrate was injected dropwise into the ZnO solution, sonicated for 1 minute, and stirred for another 15 minutes. Once done, the round bottom should be heated so the solution is at 80ºC and is kept stirring for 24 hours.
When the 24 hours are done, the solution was taken and placed in falcon tubes for centrifugation at 10 krpm for 10 minutes and the excess cobalt nitrate is then decanted. This process is done 3 times to ensure there are no excess nitrate groups left in the system. Once we have a clean product, we freeze the falcon tube with liquid nitrogen it is place in a freeze dryer to remove excess water. Afterwards, the product is collected and annealed in a ceramic boat at 300ºC for 2 hours to remove any organics left in the system. This is our final product.

CHAPTER V

RESULTS AND DISCUSSION

5.1 Band Gap Engineered Zinc Oxide Nanostructures via a Sol–Gel Synthesis of Solvent Driven Shape-Controlled Crystal Growth

5.1.1 Introduction

Manipulating ZnO has been of constant interest due to its electronic properties. Methods like chemical vapor deposition (CVD), pulse laser deposition (PLD), and molecular beam epitaxy (MBE) have been used to modify ZnO for the electronics industry in hopes of replacing GaN and other materials.[1–3] Efforts have also been made to use aqueous synthesis methods whether it be traditional wet synthesis, microwave, or sonochemical.[4–8] Organic solvents have been explored but with limited literature that modifies aqueous systems with the use of common solvents.[9,10] The ability to modify ZnO with the use of common inexpensive solvents would prove to greatly advance ZnO and its uses. Among these uses is its application for absorption with its wide bandgap of 3.37 eV for the photovoltaics industry. As mentioned in **Chapter III**, a method has been developed to address this concern. By using different solvents, they're should be the ability to achieve different morphologies by having the solvent interact with the crystal facets that are first formed at the initial growth step.[11] This will lead to highly crystalline structures that will lead to differences in bandgap. Crystallinity, morphology, chemical composition and optical properties will be explored.

5.1.2 Synthesis and Characterization of ZnO

The synthesis of zinc oxide has all been performed in a 100 mL round bottom flask. The materials used were zinc chloride of 97% purity and sodium hydroxide pellets. Combining the two materials in 30 mL of solvent and 5 ml of DI water it was stirred for 15 minutes. Afterwards it was heated to 80ºC and continued stirring for another 60 minutes before the stir bar was removed and the round bottom was capped and left at heat for 24 hrs. The precipitate was collected and washed in DI water three times by centrifuging for 10 minutes at 10 krpm. The samples were then suspended in isopropyl alcohol for further characterization. **Chapter III** illustrates a flow diagram of the procedure.

Both its rock salt and wurtzite crystal structure yield a 3.37 eV optical bandgap or 369 nm absorption with minor variation in its bulk form. Due to the nano-scaling of the material however, we should be able to see differences in bandgap due to the solvent growth effect. In Figure 5.1, we see the optical bandgap varies significantly with the solvent used during the growth process. Figure 5.1 the absorption spectra are ZnO nanostructures that have not undergone heat treatment. It is possible to assume that even after three DI water washes the solvents are still functionalized on the surface of ZnO causing such drastic bandgap shifts.

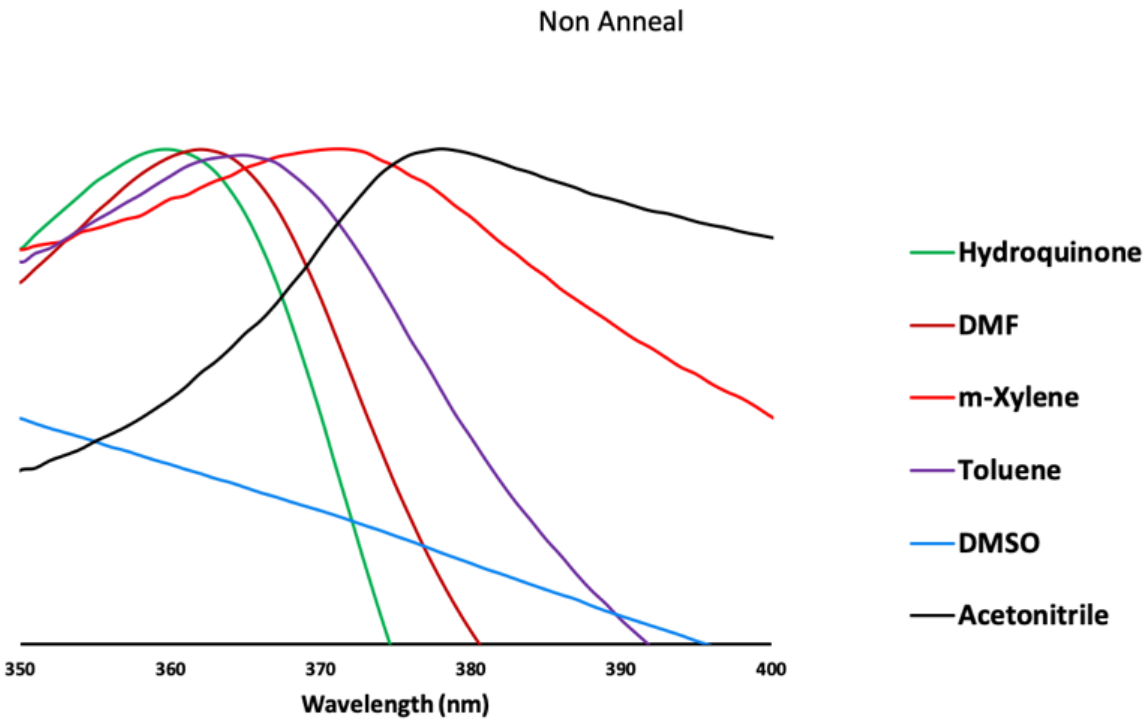

Figure 5.1. UV-Visible Spectra of ZnO Structures Synthesized with Different Solvents.

Figure 5.2 shows the absorption after annealing for two hours at 300ºC and shows a much more closely bound set of bandgap distributions from the synthesis. The choice of annealing for two hours at 300℃ was made since most organic solvents would evaporate or burn off the surface especially after two-hour mark. The obvious outlier in the dataset is DMSO. One reason for this possibility of it forming a super base with the sodium hydroxide actually preventing the growth of rods. Another way of describing this reaction is the super base never allows the nucleation process to continue to for nanostructures due to the super basic conditions. Another possibility is that due to DMSO and its large dipole, DMSO might coordinate too strongly with the Zn^{2+} forming a Zn-DMSO complex that the NaOH cannot break.

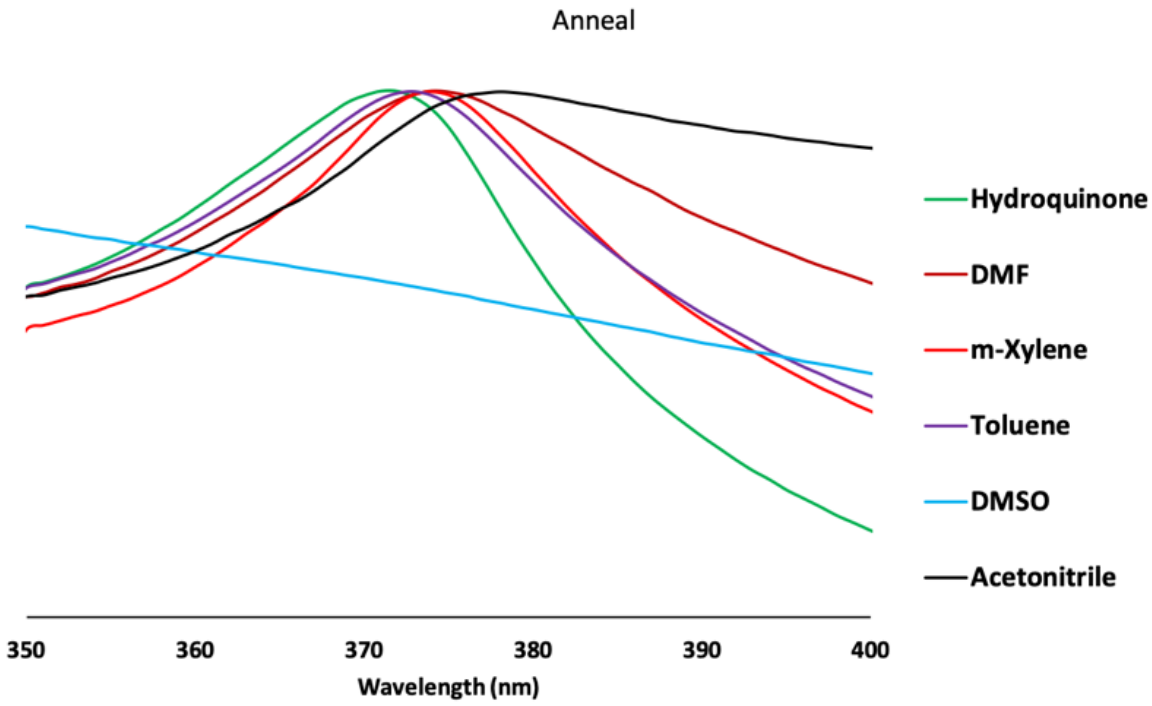

Figure 5.2 UV-Visible Spectra of ZnO Structures Synthesized with Different Solvents.

As seen with Figure 5.1, there is a fair spread of bandgap differences to bulk ZnO. The hydroquinone (HQ) is not a solvent but due to its aromaticity the presumption was it will behave like toluene and m-xylene. To mimic solvent like conditions HQ was added to DI water until it reached saturation which was 1.78 g in 30 mL of DI water. While this did give the greatest shift in bandgap it was a blue shift which was undesirable for both non-annealed and annealed samples. Comparing the non-annealed and annealed samples, it is clear that solvent binds to the surface of the ZnO causing such a bandgap difference.

The next solvent to discuss are DMF. This is an aprotic solvent with a strong dipole on top with a primary amine group that can coordinate metals. Amine groups in general (primary, secondary, tertiary) all can have profound effects on a nanoparticle

system and have led to very stunning morphologies and other qualities for applications. In literature, it is seen that HMTA, EDA, etc are used to create wonderful nanorods in solution and in films. The issue is these secondary amines are volatile and pose an overall health hazard for the user and the environment with the added benefit of being expensive. It was for these reasons DMF was chosen as a solvent.

Grouping toluene and m-xylene since they are similar in dipole and structure. If the reader asks “why not benzene?” then they have not read the SDS for benzene. Toluene and m-xylene are better since the human body has a chance to methylate the aromatic rings making them easier to handle and less toxic. Starting with toluene, the absorbance is 365 nm and m-xylene is at 374 nm. With a simple modification to the solvent a large difference occurs. It would be more accurate to look at the annealed samples to see if functionality is affecting this shift. With Figure 5.2, it is seen that there is only a 1 nm difference between toluene and m-xylene which would make much more sense in that they are both very similar in terms of structure so the ZnO would also turn out to be very similar. Note that the m-Xylene ZnO did not change its bandgap.

Acetonitrile is the last of the solvents and like m-xylene, the annealing process did not change its bandgap. This means that there was likely no solvent adhered to the surface of the nanostructures and the acetonitrile formed highly crystalline structures. Looking at bandgap though solvent alone is only part of the story. To gain further information the morphology of each system needs to be analyzed.

Each solvent system went under a SEM and TEM to undergo morphology studies. Figure 5.3 shows each nanostructure. As it can be seen, the preferred shape are hexagonal

nanorods in masse. While Figures 5.3a, b, c, and e are hexagonal rods they do show a variety of differences with the most obvious being Figure 5.3c which used acetonitrile as the solvent. Relatively large nanorods are formed with noticeable defects that spread into smaller rods. Looking at acetonitrile and how it would interact with ZnO sols, it becomes apparent that the structure is small and coordinated binding sites would not be selective for hinderance in a crystal facet for oriented attachment giving preferred growth. This results in large dimensioned rods with no inhibited growth in the a or c axis. The other three solvents that showed hexagonal rod formation were DMF, toluene, and m-Xylene.

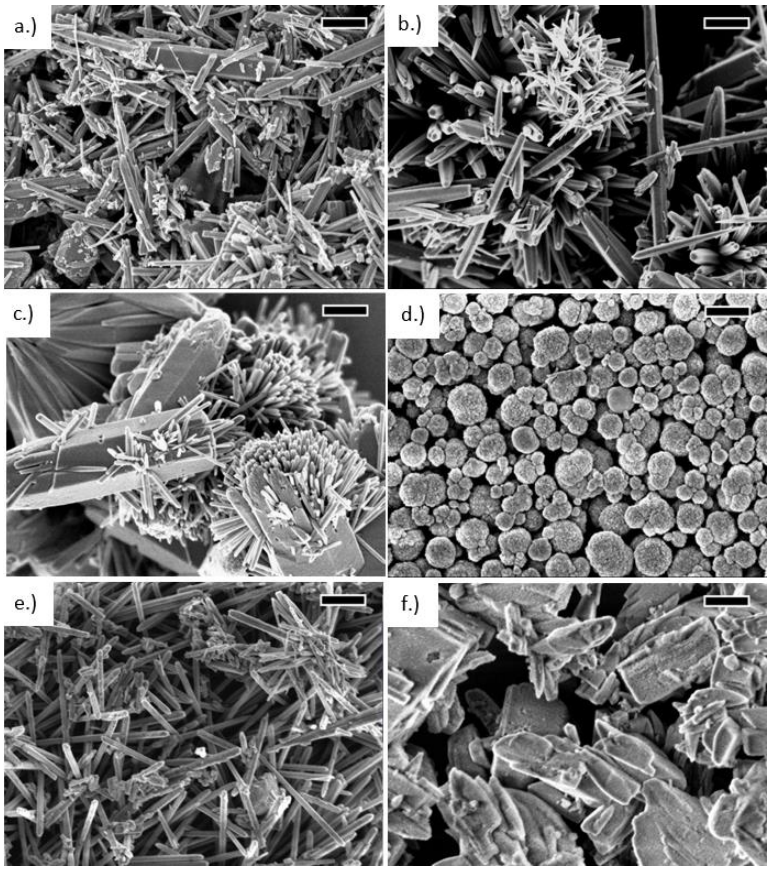

Figure 5.3. SEM Images of Synthesized Zinc Oxide. a.) m-Xylene; b.) DMF; c.) Acetonitrile; d.) Hydroquinone; e.) Toluene; f.) DMSO. Scale Bar 500 nm.

The dimethyl formamide in Figure 5.3b shows an uneven distribution of nanorods that is undesirable but as seen later with other data including the optical bandgap measurements from UV-Visible, will prove to be the best solvent to use in the system. The bifurcation shown is believed to be a homogeneity issue with stir time and mixing, specifically slow dripping the DMF and stirring until homogeneous. For m-Xylene, we see again hexagonal nanorods formed but with a range of dimensions which is certainly worse than DMF. This inhomogeneity is most likely due to the fact that m-Xylene is not miscible with water and when doing the slow drip with the solvent, the interaction is brief and not continuous resulting in such a distribution. Toluene proved to give the best morphology in terms of uniformity and great aspect ratios. With m-Xylene and toluene the UV-Visible spectra showed a well-defined peak like DMF. Like m-Xylene, toluene is not miscible with water but formed nice structures. The reason is toluene is only a little more soluble in water leading to longer interaction times with the slow drip resulting in the sols being affected by the toluene adhering to certain facets. The toluene and m-Xylene bind to the [001] and [101] crystal faces allowing the zinc oxide sols to grow into rods. As for DMF, it is likely that with such a strong pH in the system, DMF breaks down into formate and diethylamine. It is known that amine groups strongly coordinate with zinc ions and sols to form nanorods. One of the biggest reasons the use of toluene and m-Xylene was not further pursued was the product had to be washed vigorously and a lot more times than the other solvents making it disadvantageous to continue further studies.

The two that did not exhibit this feature are DMSO and HQ. As discussed earlier, DMSO acts either as a super base or as a strong detergent to zinc inhibiting growth. This

would match what the UV-Visible shows as there is no peak for ZnO. This is apparent with the textured surface of the nanoslates as those are all the nucleation crystals aggregated together. Figure 5.3f shows a haze on the surface unlike the others which is indicative to having surfactant on the surface of your material. This would further show DMSO very strongly coordinates and binds to ZnO sols on most of the crystal facets not allowing for a preferred growth path. The HQ with its spherical formation binds to the c axis orientation and only lets the [100] and [010] facets grow. Why these two solvents did not form nanorods could be explained if the surface energy of the zinc oxide is considered. To further look into the morphology and crystallinity, TEM analysis would be necessary.

Figure 5.4 shows TEM images and selected area electron diffraction (SAED) to resolve crystallinity of a single nanostructure. As one would expect, the c-axis is prominent with the nanorods laid on their sides. Accurate measurements of c-axis separation could not be performed due to the rods not meeting the dual beam or two-spot requirement for the measurements. The two-spot condition is a technique that utilizes a double tilt stage holder that allows the user to perfectly orient the nanostructure to a specific axis allowing for precise measurements and indexing. Due to the limitations of the tool, this was not achievable.

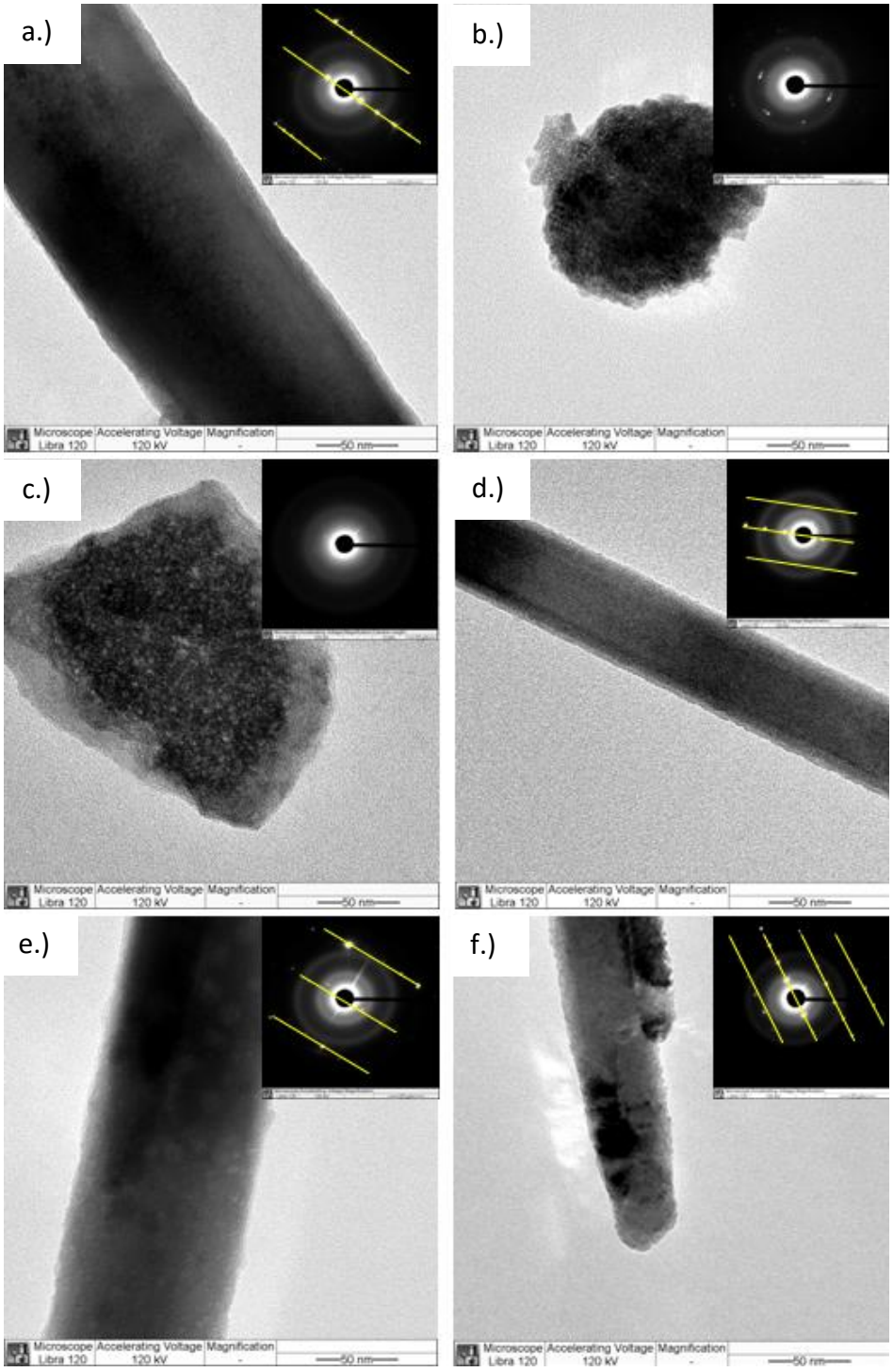

Figure 5.4 TEM and SAED Images of ZnO Synthesized in Different Solvents. a.) DMF; b.) HQ; c.) DMSO; d.) m-Xylene; e.) Toluene; f.) Acetonitrile. TEM Scale Bar 50 nm. SAED Scale Bar 5 nm-1.

As for the hydroquinone and DMSO, they show no preferential c-axis orientations. For HQ this should be expected as spherical particles should be arranged in random orientations as they lay on a surface. This allows for the SAED to show the a and b miller indices. While the SAED in Figure 5.4b may show an increased intensity in certain regions, this would not indicate a preferred growth path but simply random orientation for that specific particle. In terms of the actual image, there are nanoparticle clusters that form into these larger systems. Heavy sonication was done to see if this was a result of aggregation and the result was that these were solid features that did not break off into its individual segments. This could be a result of the HQ itself having bound to the ZnO sols, created aggregation and fused the nanoparticles together into these clusters. The DMSO shows a diffraction unlike the others in Figure 5.4c. This is due to how the particle is oriented on the surface and is simply not in a dual beam or two spot condition. This was true for all particles of this sample but clearly means that there was no preferred growth direction from the synthesis. The morphology does indicate that, like HQ, it is made of smaller individual constituents which once again indicated that there was no preferred oriented growth. As stated prior, this would also further prove that the DMSO forming a superbase, never allowing the ZnO to form into larger structures. While morphology is a strong indicator of crystallinity, all of this can be more clearly depicted through X-ray diffraction.

As seen in Figure 5.5, there are definite differences in the diffraction patterns based on solvent. This shows that the solvents affected the crystal growth and had a preferred orientation. The first three peaks are the [100], [002], and [101], respectively.

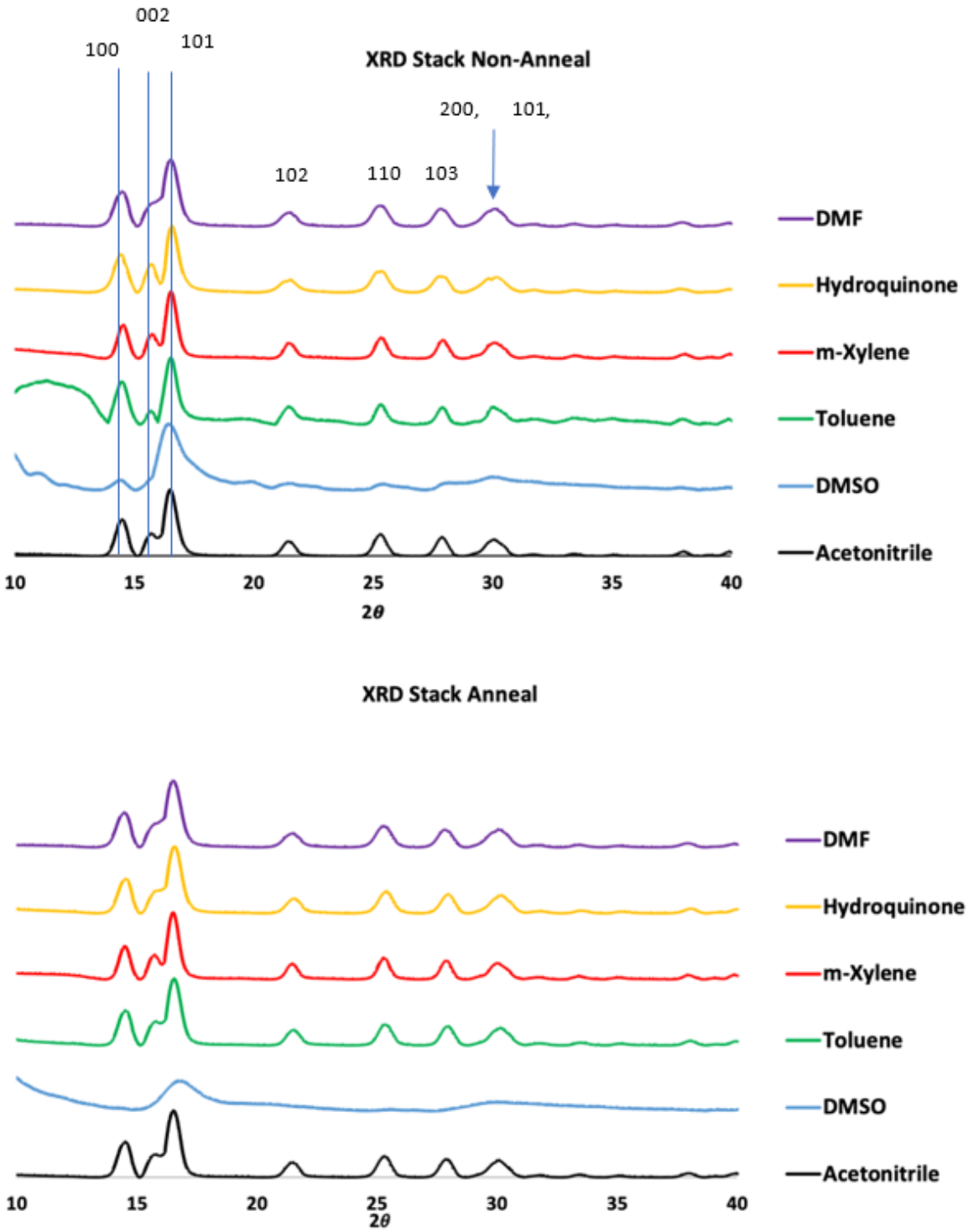

Figure 5.5 XRD Stack of ZnO Crystals Synthesized in Different Solvents.

The two peaks that are consistent with all of them are the [100] and [101] peaks. The first thing that is noticeable are the different intensities of the three main peaks. More specifically, even though the growth of four of the six nanostructures had a preferred growth of the [002] c-axis, that is the least intense peak. This is actually to be expected since XRD is essentially averaging all the particles within the scan area. Observing SEM images specifically, if the ZnO rods are in clusters then the [100] and [101] crystal orientation would be more exposed since the sides have more surface area than the top and bottom of the hexagonal rod. By looking at the [002] peak we see variance in intensity and even in the 2θ spacing from the [101] peak. Through annealing, we see the crystals relax and see the three that changed the most were HQ, toluene, and DMSO. One thing to note is annealing does remove residual organics that are adhered to the surface giving a clear diffraction. This held especially true for the toluene sample as seen between the 10 – 14 2θ angle where that region is the detection of carbon, or rather contaminant. This could also be the reason why, especially for toluene, the [002] peak was not well resolved due to organics. Moving back to DMSO, once again it is the outlier in the set. The [100] is noticeable and the [101] positions but not the [002]. On top of that the (101) has a larger FWHM than the rest which indicates that the crystal grains are incredibly small indicating that there was no growth to the nanostructure regime. This is further proof tied with the TEM images that the ZnO sols never formed in an oriented growth fashion After annealing, the [101] peak intensity actually gets worse and a loss of the [100] peak is observed. This could be due to the phenomena of as a material gets smaller the melting point decreases as well. This is well known with gold being a prime

example. Essentially, then annealing treatment actually made the ZnO system more amorphous. With this and all other characterization thus far, it can be said with confidence that DMSO is not a compatible solvent for our system.

Comparing the XRD between the other solvents, it is seen that there are discrepancies. The only solvent that did not undergo any peak shift is the DMF after the heat treatment. For HQ and Toluene, we see an increase to intensity in the [002] peak as well as that same peak converging into the [101] peak. This would normally mean that the grain size would be decreasing if the FWHM was increased but that is not the case in this situation. The [002] peak after annealing simply shifts a greater amount to a larger 2θ than the [101] peak. This would normally mean that the c-axis is more exposed to the X-ray causing stronger diffraction but once again, it is suspected that organic residue from the HQ and the Toluene masked the [002] peak in terms of intensity. Organics would not result in giving a false peak shift since it would not be part of the crystal lattice. The only other solvent that had a unique change was m-Xylene where the 2θ position contracted rather than expanded like the rest of them. For the DMF and acetonitrile system it can be seen that in both 5.5a and 5.5b the [002] and [101] peaks are somewhat fused together. This is a consequence of using the Molybdenum source which does not have the same resolution as a Copper source. Furthermore, there was no correlation between peak shifts and bandgap shifts after annealing which verifies that the solvent was acting like a surfactant causing wide bandgap shifts. All XRD were taken with the same parameters so no variation due to instrumentation should have occurred.

XPS was performed on the ZnO sol before heat was applied as well as ZnO with m-Xylene and DMSO. The ZnO sol was washed the same way as the precipitate was done to remove the solvent and the salts that may have been formed. This worked since the survey shows now sodium, chlorine, and sulfur indicating that at least the salts have been removed as shown in Figure 5.6. sodium, chlorine, and sulfur indicating that at least the salts have been removed as shown in Figure 5.6.

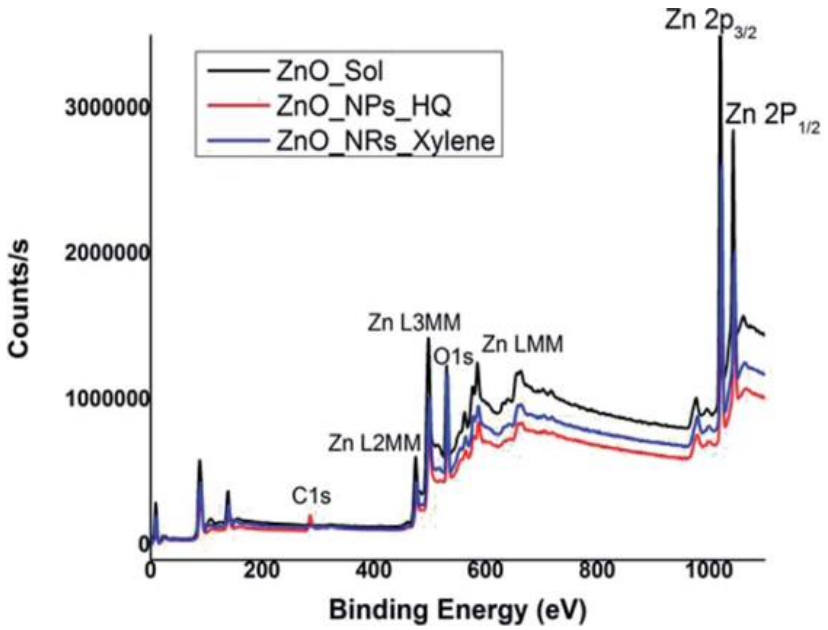

Figure 5.6. XPS Survey of Zinc Oxide System of ZnO Sols, ZnO Synthesized with HQ and m-Xylene.

In the single element scans we see that the raw spectra are shifted from each other. While this is very important for XPS it is imperative to understand that we need a reference source. It is typical to use adventitious carbon as a reference source. Adventitious carbon is essentially unavoidable carbon contamination from the samples

being exposed to atmosphere which results in a 1-2 nm film on the sample. In literature the C-C bond is used at 284.8 eV. Therefore, any sample that does not have a C-C binding energy of 284.8 eV needs to be given a charge shift as a correction that will also affect the other single element peaks in that spectra. In this case it is possible that the carbon bonds are also due to solvent being adhered to the surface of the particles.

Starting with the ZnO sol system in Figure 5.7, the C-C bond is measured at 283.8 eV so it is necessary to shift the oxygen and zinc peaks by 1 eV from their reading. This gives the oxygen 1s peak at 530.1 eV with the shoulder peak at 531.1 matching nicely with a metal oxide peak and metal carbonate species, respectively. the zinc $2p_{3/2}$ peak being at 1021.3 eV and this is actually 0.7 eV lower than expected if this were ZnO, but recall that these are the sols before growth. Therefore this is an indication that this peak is actually a mix of $ZnO/Zn(OH)_2$. With the hydrogen attached and it being far less electronegative, it makes sense that the zinc peak would have a lower binding energy that normal ZnO.

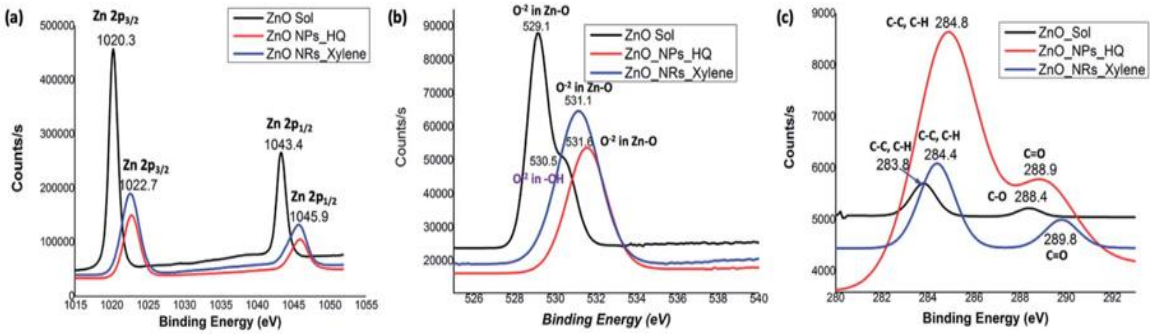

Figure 5.7. XPS Individual Scans. a.) Zinc; b.) Oxygen; c.) Carbon.

Moving to m-Xylene, there is only a shift of 0.4 eV from the C-C peak. This would place the oxygen peak at 531.5 eV and the zinc at 1023.1 eV. The oxygen peak is in the regime of metal carbonates which is something we would definitely expect with ZnO being synthesized with organic solvents. Due to the rapid growth of sol-gel synthesis, carbon could embed inside the ZnO crystal causing defects and/or metal carbonates to form. This is also where C=O bonds would appear however, which would appear in the presence of adventitious carbon and is seen in the carbon scan.

Finally, the HQ was the only one that had no charging effects and the single element scans can be taken at face value. The higher intensity count for the carbon scans would suggest that HQ is on the ZnO surface more so than the m-xylene as a surfactant. This would make sense and explain why the ZnO formed particles instead of rods.

Electrical conductivity measurements were performed on the zinc oxide system as well as the sols and for comparison a thin films system made of ZnO rods. The thin film zinc oxide nanorods were made by spin coating ZnO sol onto a film several times to build up a sufficient thickness before growth. The film was then place in a DI water bath with zinc nitrate and ethylene diamine for 1.5 hours at 80ºC. Afterwards, gentle sonication was applied to remove excess ZnO particles not attached to the surface so that conductivity measurements could be performed only for the film. As shown in Figure 5.8, a two-probe measurement was done with 100 nm of copper deposited as the contacts. Figure 5.8b shows that the ZnO NR film performed the best in comparison to the sols by an order of magnitude. This makes sense seeing how there are no breaks or short circuits present allowing current to flow uninterrupted.

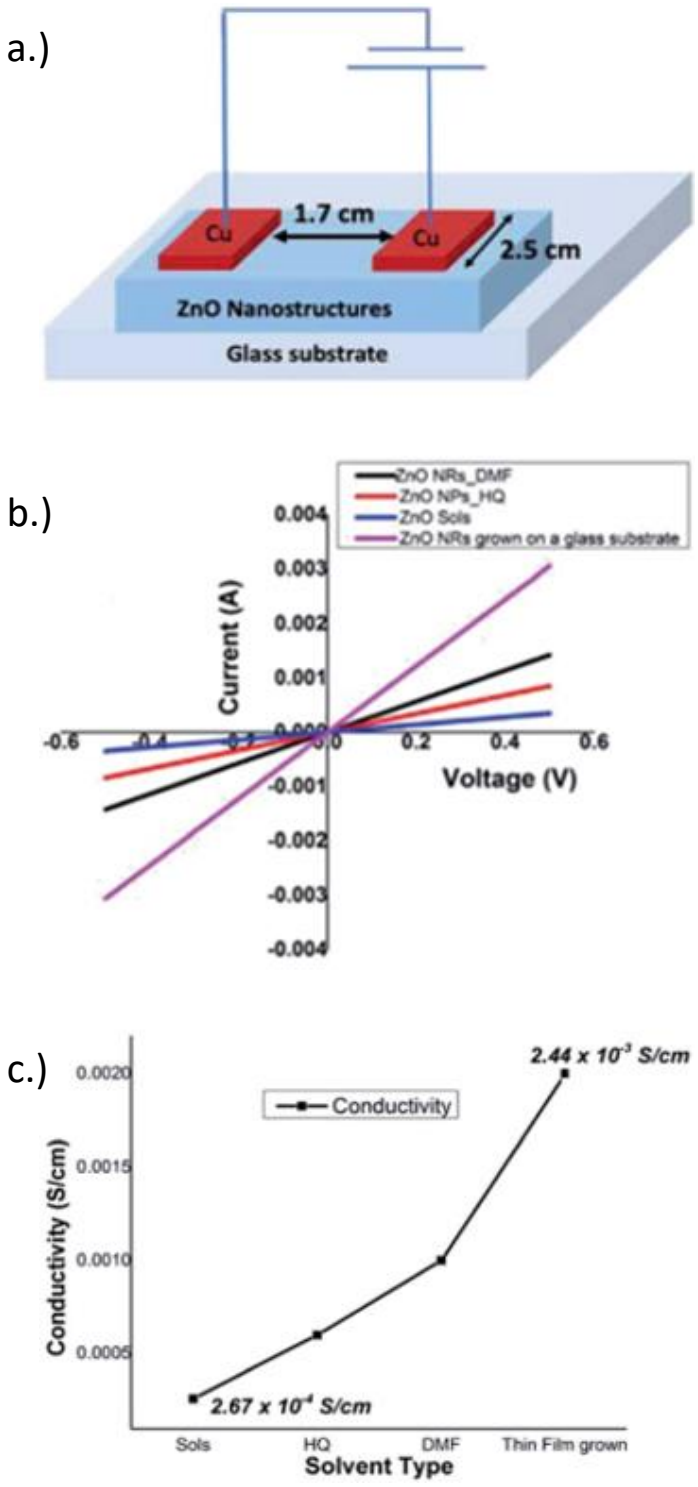

Figure 5.8. Diagram of Measurement Procedure with Conductivity Measurements and Trends.

The DMF, HQ, and sol solution did not perform as well as expected since the DMF and HQ was done via spin coating. As for the sols, the hydroxyl groups associated with the zinc plays a major factor in loss of conductivity. In fact, from sol to NR thin film an order of magnitude difference is observed showing not only uniformity is a major factor but also nanorods systems seem to perform better than other nanostructures. It is for this reason this dissertation proceeds to use DMF-based nanorods for the rest of the chapter. While the m-xylene and toluene would have also been acceptable, the confidence of removing nonpolar solvents proved challenging.

5.2 ZnO Doping

5.2.1 Introduction

Doping can play a huge role in changing desired properties with optoelectronics in mind. Whether through intrinsic or interstitial placement of a dopant atom, added strain on the crystal induces a change in orbitals overlapping that causes a shift in bandgap, fermi level, conduction and so on. This manipulation of material can prove advantageous to our system and to extend the concept, the choice for the synthesis is to see if doping can have a greater affect if a different solvent system is applied. As seen earlier in the chapter, solvents can drastically affect the morphology of the system by binding to crystal facets. An extension to this result is by using different solvents to coordinate the dopant along with the zinc, incorporation of dopant material should be increased to further optoelectronic properties. The other thing that would change is based on dopant level and solvent, new morphologies could occur in the presence of other metals. This would be due to the interaction of the solvent guiding certain crystal facets

of the sol to give a preferred direction of growth. This would be different from exclusively having zinc oxide since there is more coordination bonds with different geometries due to the unfilled d orbitals in the other first row transition metals.

5.2.2 Synthesis and Characterization of Doped ZnO

The typical procedure that was followed was closely followed the synthesis procedure in Aim1. The only difference is the dopant metal was introduced at the same step that zinc chloride and sodium hydroxide were mixed. Ratios would vary volume to volume of Zn:M with 1-10% of the dopant metal to the zinc. All syntheses were done at 24 hours and ranged from 80℃ to 140℃. Anhydrous zinc chloride was used as the zinc source when the dopant precursor was also a chloride. Zinc acetate was only used for erbium trifluoroacetate and copper acetate. Prior results show that the zinc oxide synthesis using zinc acetate showed no difference in nanorod formation. The only difference when using the acetates is that extra washes are necessary to remove byproduct from the reaction.

The ability to dope is dependent on synthetic scheme. Both metal precursors must be mixed well together before introducing DMF as the main solvent. This is because metal ions must be homogeneous throughout before the sol process to take place from the NaOH. Once a proper mix has happened adding the nucleophile should induce dopant material as the sols form. Remember, the solvent binds to the crystal facets in the sol phase in order to determine the morphology of the system so thorough mixing is essential. Mixing metal precursors separately and then introducing the sodium hydroxide would result in two different morphologies for the final product. Dispersing the zinc

chloride and the dopant in the DMF before water and sodium hydroxide is introduced would also cause problems. The metal atoms would coordinate with the DMF before the sol is formed causing no growth to form or at minimum inhibit growth.

As previously mentioned, one of the main reasons to dope a material is to change its optical and electrical properties to be applied to a certain system. Looking at a UV-Visible spectrum, determining optical bandgap is possible. In Figure 5.9 we use the ZnO synthesis of DMF as a reference where the peak is at 362 nm. The results are desirable. All dopants caused zinc oxide to red shift where in the application of photovoltaics this is needed. Strangely enough, all of the dopant peaks are only within two nanometers of each other. However, when XRD is examined the crystal structure of zinc oxide has not been significantly modified.

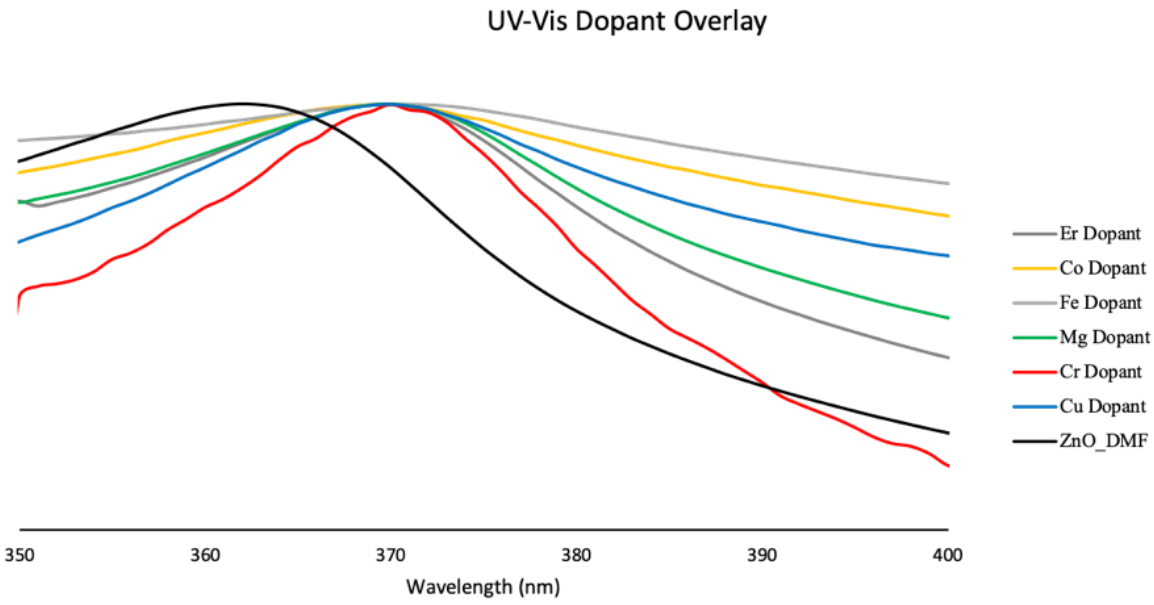

Figure 5.9. UV-Vis Comparison of Peak Positions between Dopants.

Unlike the core shell system, X-ray diffraction can be done to verify changes in the crystal structure as an initial insight. What is expected is to see are shifts in the main three peaks optimistic however seeing a couple tenths would show that doping has occurred. In Figure 5.10 the step size used for the XRD was roughly 0.015 theta so any peak that deviates from the original peak would be considered successful doping. Extra peaks are an indication that dopant structures have been formed showing a bifurcation in the synthesis and as this dissertation will show, different morphologies. Of the dopant materials, extra peaks are seen in the copper, chromium, and iron diffraction while magnesium, cobalt, and erbium maintain a wurtzite structure without any additional peaks.

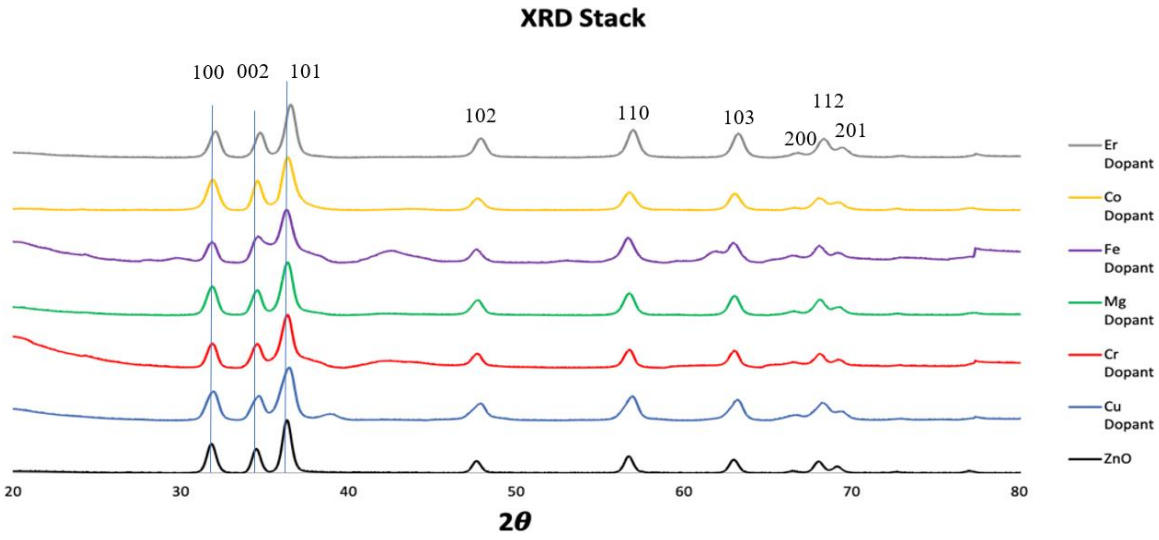

Figure 5.10. XRD of ZnO and ZnO dopants.

All dopants produced a shift but copper, cobalt, and erbium are the dopants that produced the largest shift in ZnO three main peaks with erbium having the biggest effect

then copper and then cobalt. Erbium produced a 2θ shift of 0.25, copper with 0.13, and 0.09 for cobalt. This makes sense just due to the ionic radius of each material and that when incorporated into the wurtzite lattice would cause a larger shift based on size.

Out of all the dopants, iron was by far the worst. This is probably due to how iron like to form a non-hexagonal structure. Also, it was the smallest ionic radius out of all the dopants showing that choice of material is not solely based on valency. Chromium and erbium both with a 3+ valency saw moderate success. Even though erbium is a heavy element, its ionic radius is closer to zinc which is a reason that it was able to pair better.

The ability to dope is dependent on synthetic scheme. Both metal precursors must be mixed well together before introducing DMF as the main solvent. This is because metal ions must be homogeneous throughout before the sol process to take place from the NaOH. Once a proper mix has happened adding the nucleophile should induce dopant material as the sol forms. Remember, the solvent binds to the crystal facets in the sol phase in order to determine the morphology of the system so mixing is essential. If not done, different morphologies will emerge and also different crystalline structures as seen in the XRD.

SEM analysis showed that there were different morphologies within the same synthesis batch which was initially indicated by XRD. Figure 5.11 shows different morphologies of just one synthesis using copper as the dopant material. This particular synthesis had a 1:10 ratio of copper to zinc atoms which is a large amount of dopant. However, this did lead to morphologies that have not been reported. Specifically, in Figure 5.11e, there are chain-like structures make from connected nanorods giving a

hierarchal structure. In 5.11f is a less magnified micrograph of 5.11e to show that these structures actually link with each other giving it two orders of hierarchy. While goal of this research is to dope and maintain nanorod formation, this is an exciting find. The possibility of creating hierarchal structures based on precursor rather than more complex, exotic methods. It should be mentioned that the dominant morphology was Figure 5.11a with the other images be scarce on the prepared sample.

In Figure 5.12 we see how introduction of dopants affect the morphology of a known synthesis. For this synthesis system, zinc oxide should form into nanorods. What is seen are different morphologies not just between the dopants but within the same image. Chromium as the dopant was the only one that had one homogeneous structure. Upon closer inspection for erbium and iron, the nanorods are littered with nanoparticles with iron also having plate structures in the background. This is an indication of four possibilities with the first being that when the initial mixing was done, the zinc chloride only formed into zinc sols and the dopant formed its own without being included into the zinc sol. The second is the zinc sol did form without the dopant material and in another localized area zinc sol formed with the dopant metal leading to nanostructures other than nanorods. The third being the zinc oxide was doped when we see the nanorods and at local areas where dopant was a little more predominant, zinc oxide was heavily doped to form other morphologies. Finally, the zinc oxide was doped but based on kinetics, the dopant metal formed sols before being included into the ZnO giving different structures.

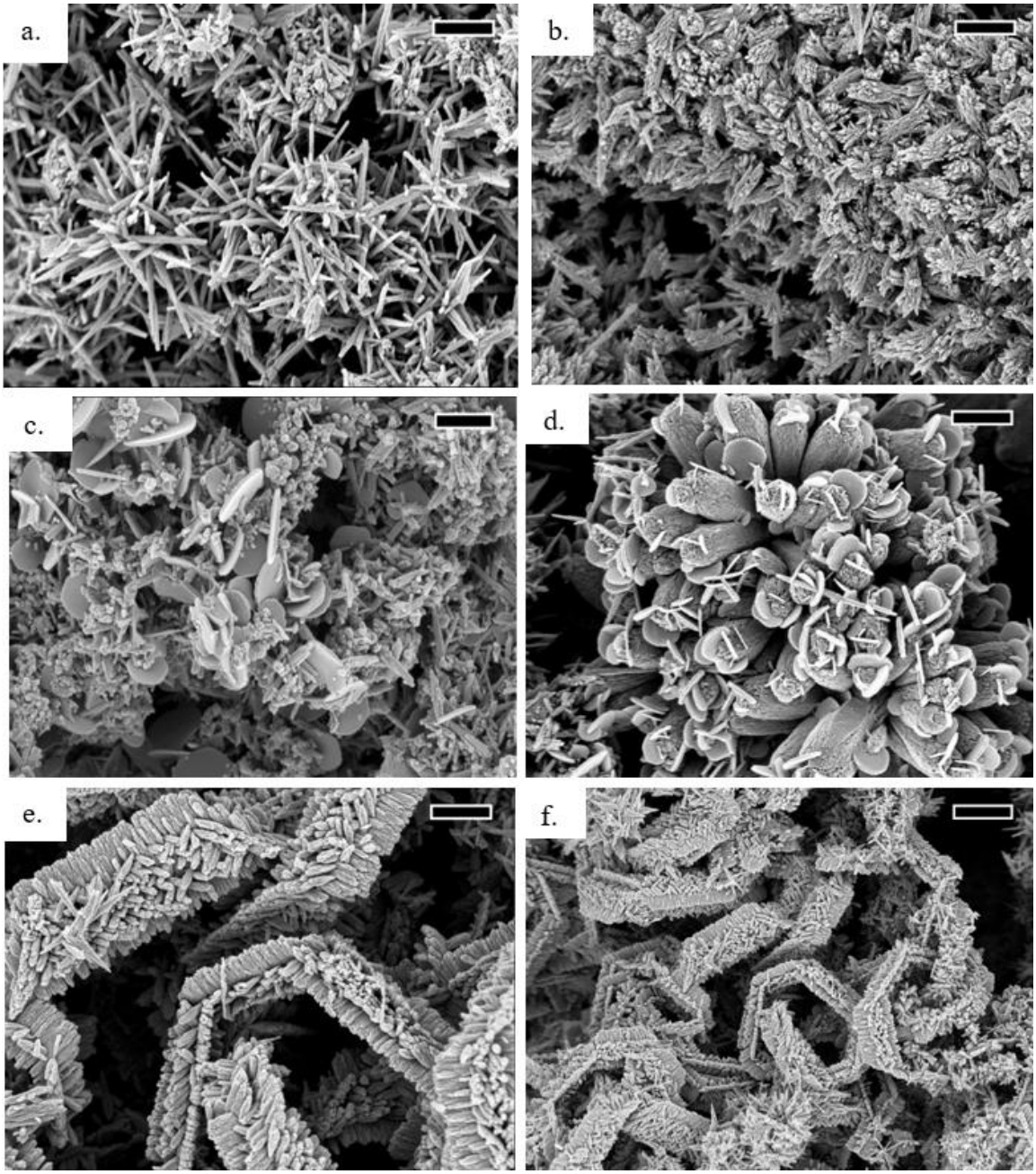

Figure 5.11. SEM Images of ZnO with Copper as the Dopant Material. Micrographs a-e Have a Scale Bar at 500 nm. Micrograph f has a Scale Bar of 1μm.

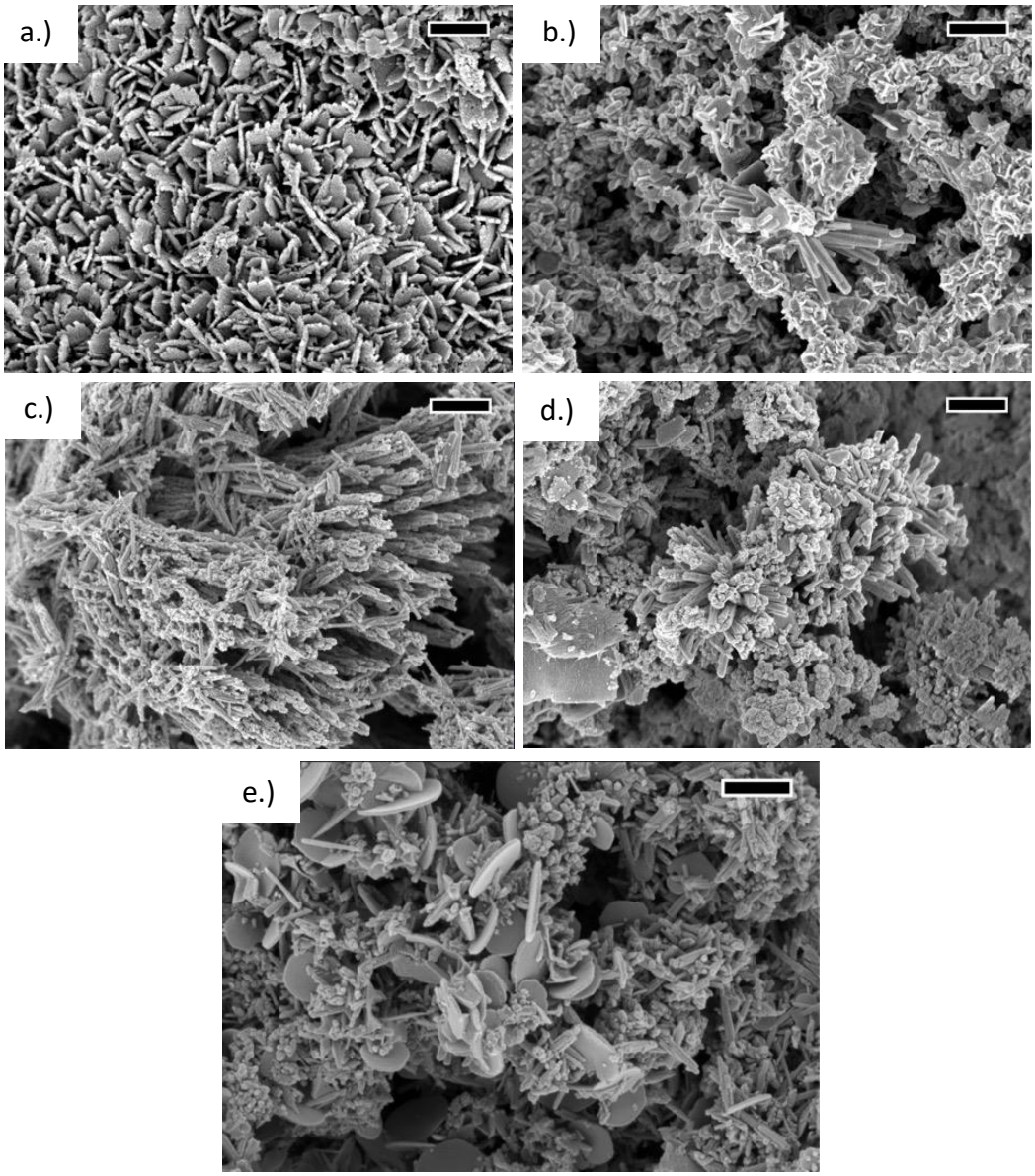

Figure 5.12. SEM of ZnO with Different Metal Dopants. a.) Chromium; b.) Magnesium; c.) Erbium; d.) Iron; e.) Cobalt. Scale bar 500 nm.

Comparing with XRD, the third and fourth options are the most likely since for some of the patterns are very clean with the wurtzite structure with a shift in the two-theta spacing while other patterns did include extra peaks. The UV-Vis also shows that the zinc

oxide has been doped but looking at the onset of the peak as well as the drop off, it is seen that there are other absorptions happening around the peak.

5.3 ZnO:CoO Core-Shell Nanostructures

5.3.1 Introduction

One common use for ZnO is how it can be manipulated to change its optical bandgap. These methods are conventionally done by either doping or core/shell methods with each having their advantages. Doping is usually the preferred process when tuning bandgaps due to its effectiveness and ease. Core-Shell systems have the advantage of being incredibly tunable and with certain systems can span the entire visible range which is useful for photovoltaic applications. The main problem with this method is that it typically requires expensive chemicals and typically high heat. It can also be quite a challenge controlling these nanoparticles in terms of size and shape.

Cation exchange is a very unique method in that it typically works on the principal of kinetics and thermodynamics. The kinetics are in line with the crystal growth with the presence of coordinating ligands whereas in thermodynamics often deals with the phase and chemical composition of the material. This process essentially saturates a solvent system to the point which the shell precursor is enthalpically more favorable to the surface of the ZnO. This would force a metal precursor to replace zinc ions on the surface and penetrate within a certain depth into the material. Therefore, there is no need for exotic chemicals, high temperatures, or unwanted secondary morphologies in the system. This process has multiple advantages with the first being there is no need for bases or acids to catalyze the reaction. The second is the ease of the synthesis itself being

strait forward and finally the system is completely in water (green). While one of the best examples of cation exchange is the PbSe/CdSe nanocrystal system, there has not been a lot of work with ZnO and other first row transition metals. Here, we describe a facile way to make core/shell systems with the cation exchange process. ZnO nanorods (NR) were made via sol-gel as the core and cobalt nitrate as the precursor in varying concentrations to make a cobalt oxide (CoO) shell.

5.3.2 Synthesis and Characterization of Core-Shell ZnO

As stated previously, the ZnO was synthesized as discussed in **Chapter III**. Cobalt (II) Nitrate hexahydrate was used as the precursor material and was used in different concentrations. The choice of this precursor vs $CoCl_2$ or any other is the other ligands did not degrade under 100ºC. Note that $Co(NO_3)_2$ hexahydrate degrades at 74ºC but the anhydrous form is at 100ºC. That makes it perfect for an aqueous core-shell system. An important note is that the degradation of the cobalt nitrate is very important. There were film structures at the surface of the ZnO but this was residual $Co(NO_3)_2$ that had not reacted. This was apparent since the precipitate had a pink tint from the mix of white zinc oxide and red cobalt nitrate. At first the synthesis was done at 80ºC for 24 hours and we saw no changes on the surface of the zinc oxide even though we did detect cobalt with XPS. It was not until the system went longer than 24 hours or was set at a higher temperature that it accelerated the process. This resulted in a brownish solution. Anytime there is a color change is always a good indication that a reaction happened. The formation of cobalt oxide particle had formed on the surface of zinc oxide nanorods. This

was repeated three times and yielded the same result. Characterization was done to first identify what oxidation state the cobalt had formed.

Optical bandgap studies were performed to check for applicability towards photovoltaics. Results showed in Figure 5.13 that 5:1 w/w cobalt(II)nitrate to ZnO NRs and 10:1 w/w cobalt(II)nitrate to ZnO NRs there is a blue shift in the optical bandgap. More noticeably by annealing the system at 300ºC for two hours the optical bandgap shifted again even more so than with the solvent study alone. Even though the concentration of the cobalt(II)nitrate doubled in the system, the peaks did not change showing there could be a saturation point in the system. However, this shows that using a modified sol-gel method for a core-shell system is viable and worth further investigation.

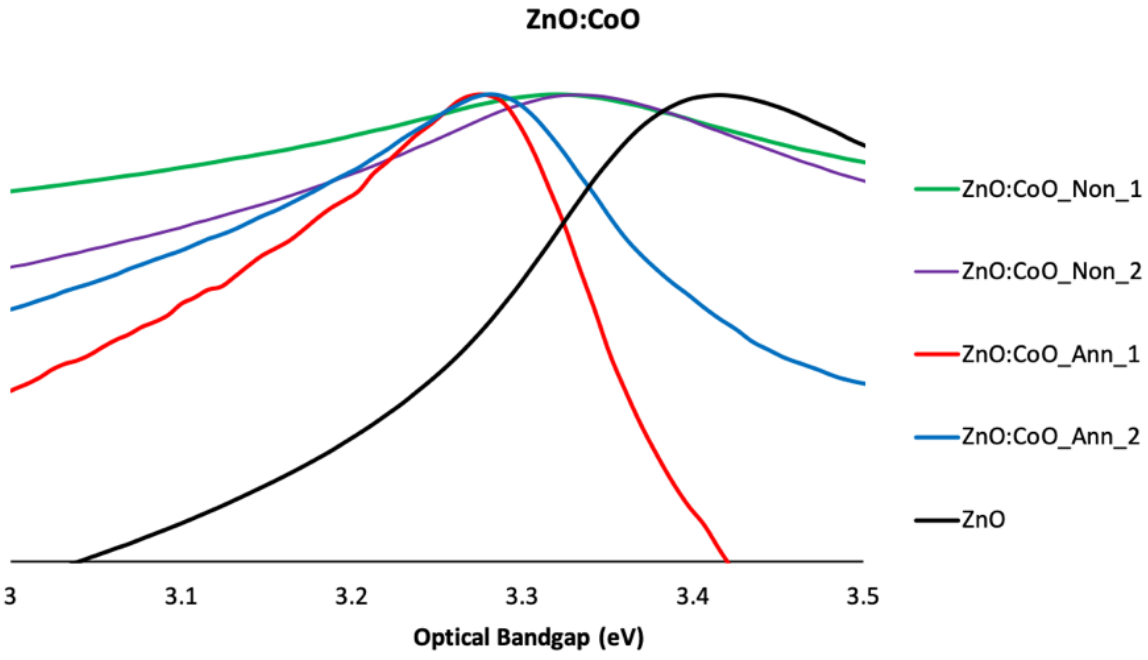

Figure 5.13. UV-Visible Spectra of ZnO:CoO System at Different Concentrations.

Crystallinity studies were done using X-ray diffraction using a copper source and would prove to be useful for determining crystal structure. There are three forms of cobalt to be expected from the system with them being CoO, Co_2O_3, and Co_3O_4. Cobalt (II) oxide is a hexagonal phase while and cobalt (III) oxide is face-centered cubic structures that are easily identifiable from each other. Something to keep in mind is the amount of cobalt oxide with respect to the zinc oxide in a powder sample. XRD as a technique could determine the crystallinity of cobalt oxide it would need to be an appropriate amount within the system. This technique can detect approximately 1-3% depending on the quality of the system. Figure 5.14 shows there is no difference between regular zinc oxide and zinc oxide with cobalt introduced. The zinc oxide that is being compared is the same synthesis batch that was used to create the core/shell system seen to the right. This result is to be expected since the shell material will be on the order of < 2 nm where the core is between 50 – 200 nm in length. It is worth noting that the peak intensities after the first three main peaks are abnormally large. This was a malfunction in the XRD where a setting was changed so that the higher two theta angles were scanned twice as long, which gave similar intensities to the main peaks. Of course, there could be no incorporation of cobalt in the system so another technique is needed to confirm the presence of cobalt. Hence, XPS was used to confirm the presence of cobalt and to find its chemical state.

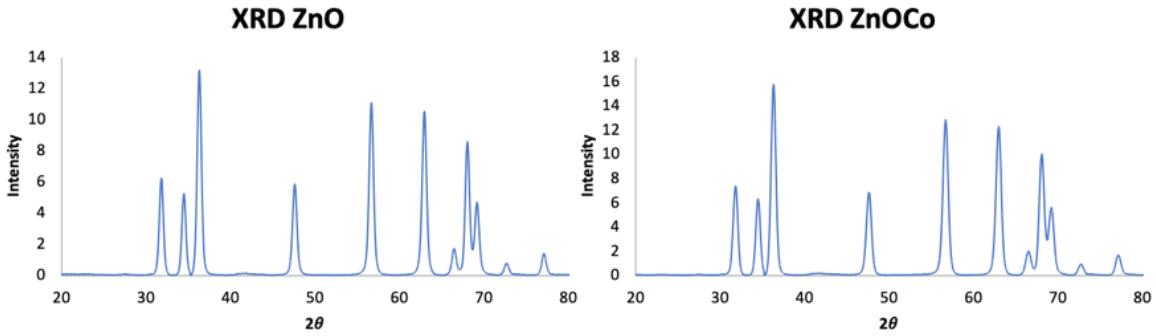

Figure 5.14. XRD of ZnO and ZnOCo Showing No Peak Shift or Extra Peaks.

XPS showed anywhere from 1-6% of cobalt depending on concentration and that is within a 10 nm penetration depth and not the entirety of ZnO rod. Therefore, the cobalt in the system is far less than 1% and would not show in XRD. Figure 5.15 gives the ZnO:CoO survey with well-defined peaks for zinc and cobalt with zinc having no change from literature.

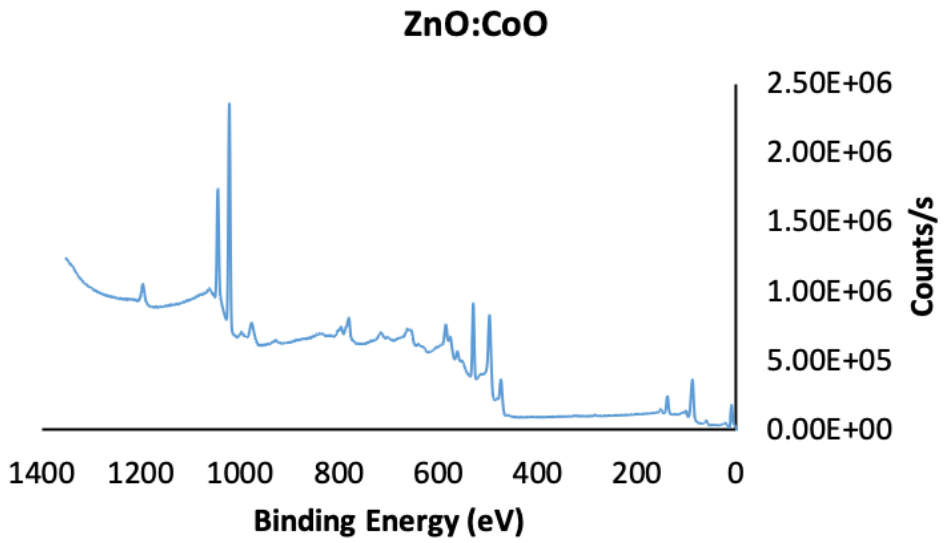

Figure 5.15. XPS Survey of ZnO:CoO Nanorod.

The Zinc values in Figure 5.16c show peaks at 1022 eV and 1045eV with the oxygen having 529.5 eV metal oxide peak with a 531.3 eV metal carbonate peak. This is to be expected since 12% carbon was present in the system. The cobalt percentage was approximately 6% with Figure 5.16a with cobalt showing that two different oxidation states do not change the main peak positions. The way to confirm if cobalt is Co^{2+} or Co^{3+} is to look at the satellite peaks. Figure 5.16a shows the difference where the blue signal has the satellite peaks further away from the main 2p peaks at 792 eV and 804 eV. In the black signal there is a noticeable change in satellite position with a 2 eV shift respectively to each peak. These spectra were obtained on the same sample and argon etching was done to get the two different spectra. Special consideration must be taken otherwise the system could change and could cause bad data. If samples are left in ambient conditions, CoO will form Co_3O_4. If this happens, using an argon etch is sufficient to remove the Co_3O_4. However, under an argon beam and in the presence of carbon, cobalt can change its chemical state into a cobalt carbide and reduce the cobalt oxide signal. Another thing to point out is that the $3p_{3/2}$ peak has slightly broadened, this is due to a mixed state of Co^{2+} and Co^{3+} and is generally unavoidable. In our system there will always be carbon.

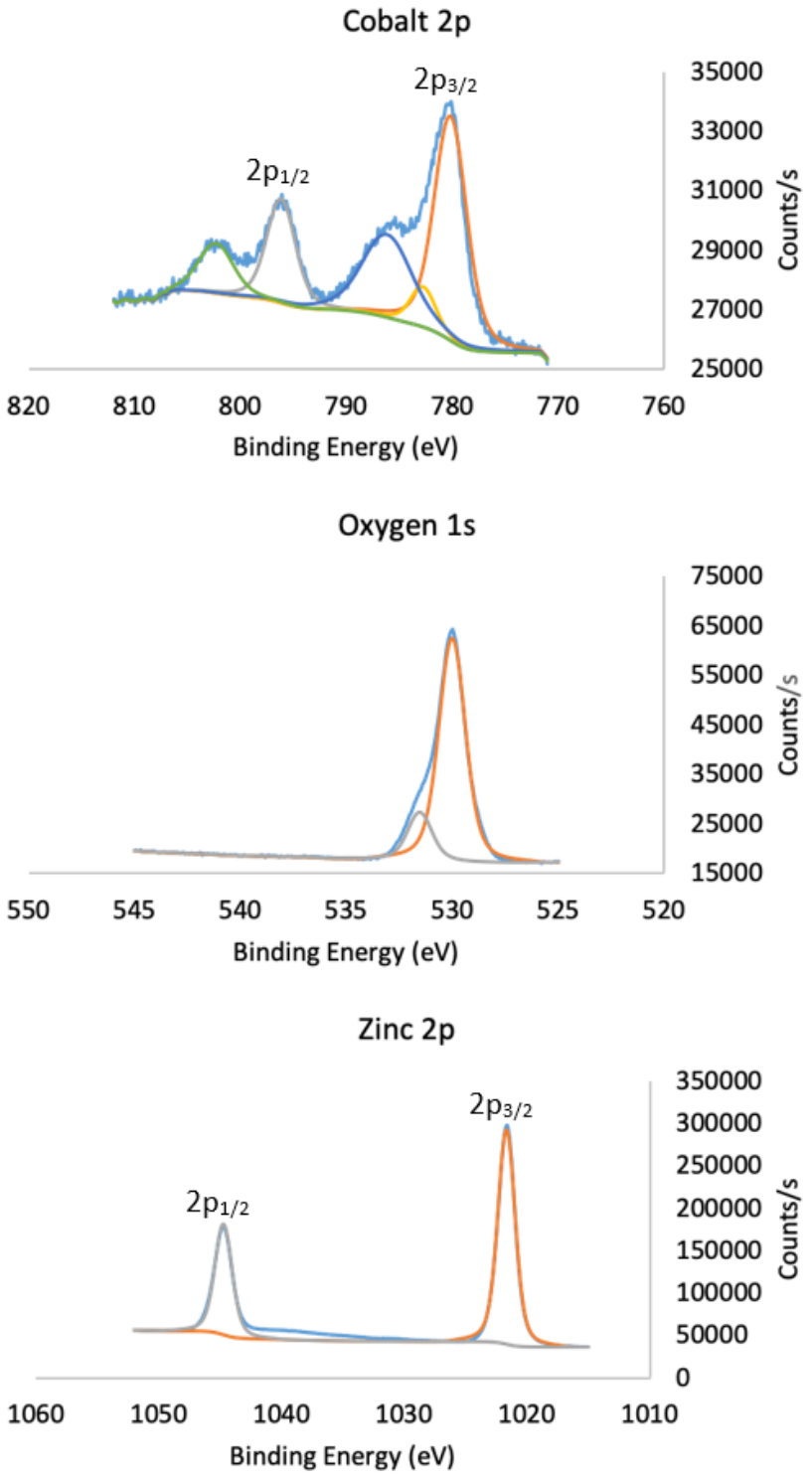

Figure 5.16. XPS Single Element Scans of Cobalt, Oxygen, and Zinc with Deconvoluted Peaks.

Figure 5.17b illustrates how an argon beam can damage and convert the CoO system into cobalt carbide by referencing peaks at 778 eV and 793 eV. Therefore, using low energy, large area etches are recommended to eliminate these situations. Carbon was used as a reference point to adjust for charge drift in the scans and the C-C 284.8 eV peak was used. It is worth noting that there was no nitrogen present in the system indicating the cobalt peaks are not associated with the cobalt nitrate from the starting material. The Cobalt peaks are shifted to a higher binding energy due to the zinc having a higher electronegativity causing this to happen.

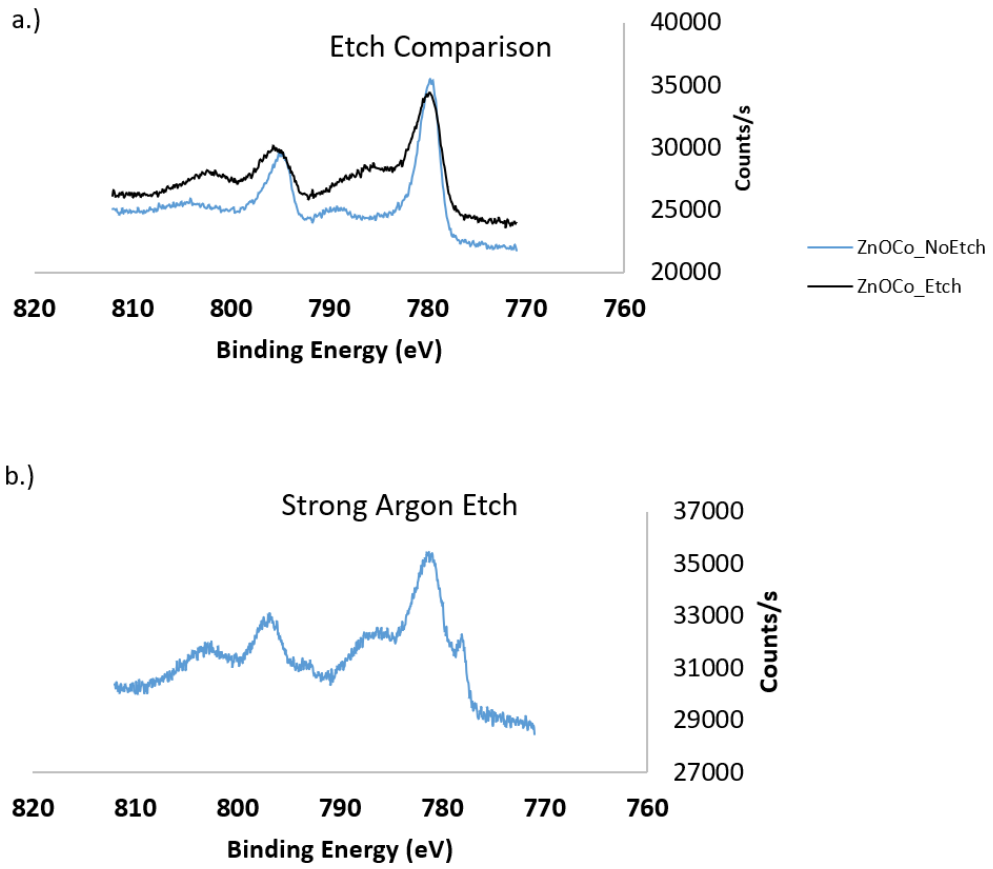

Figure 5.17. XPS Showing Possible Etching Outcomes for Cobalt Oxide. a.) Co_3O_4 to CoO and; b.) Cobalt Reducing to Cobalt Carbide.

The morphology of the system after the reaction occurred did not change the zinc oxide. Depending on the ratios we see films formed quite heavily on the ZnO NRs. At first the synthesis was done at 80ºC for 24 hours and we saw no changes on the surface of the zinc oxide even though we did detect cobalt with XPS. It was not until the system went longer than 24 hours or the temperature was raised higher that we saw results and accelerated the process. When this occurred, particle formation happened on the surface of the ZnO. A hypothesis can be formed that certain sites on the ZnO rods are more likely to bind than other possibly due to the ZnO have too many oxide layers in localized regions. This would be why particle formation occurs rather than a shell layer. With that, it would be best to stop the sol-gel synthesis before the 24 hours to wear oxide formation on the surface does not occur. This can be seen in Figure 5.18a where films are being formed on the surface orthogonal to the c-axis of the nanorods. This shows that the cobalt oxide formation does have a preferred binding orientation to the ZnO NR's and that it is incorporating to the ZnO surface. This morphology was made with the 80ºC while in Figure 5.18b still shows these films but also with nanoparticles on the surface and was made at 90ºC. As stated, the cobalt nitrate degrades at 90ºC allowing particle formation to happen instead of films. In the XPS results, there is no nitrogen present so these films are not residual cobalt nitrate where TEM shows the same result.

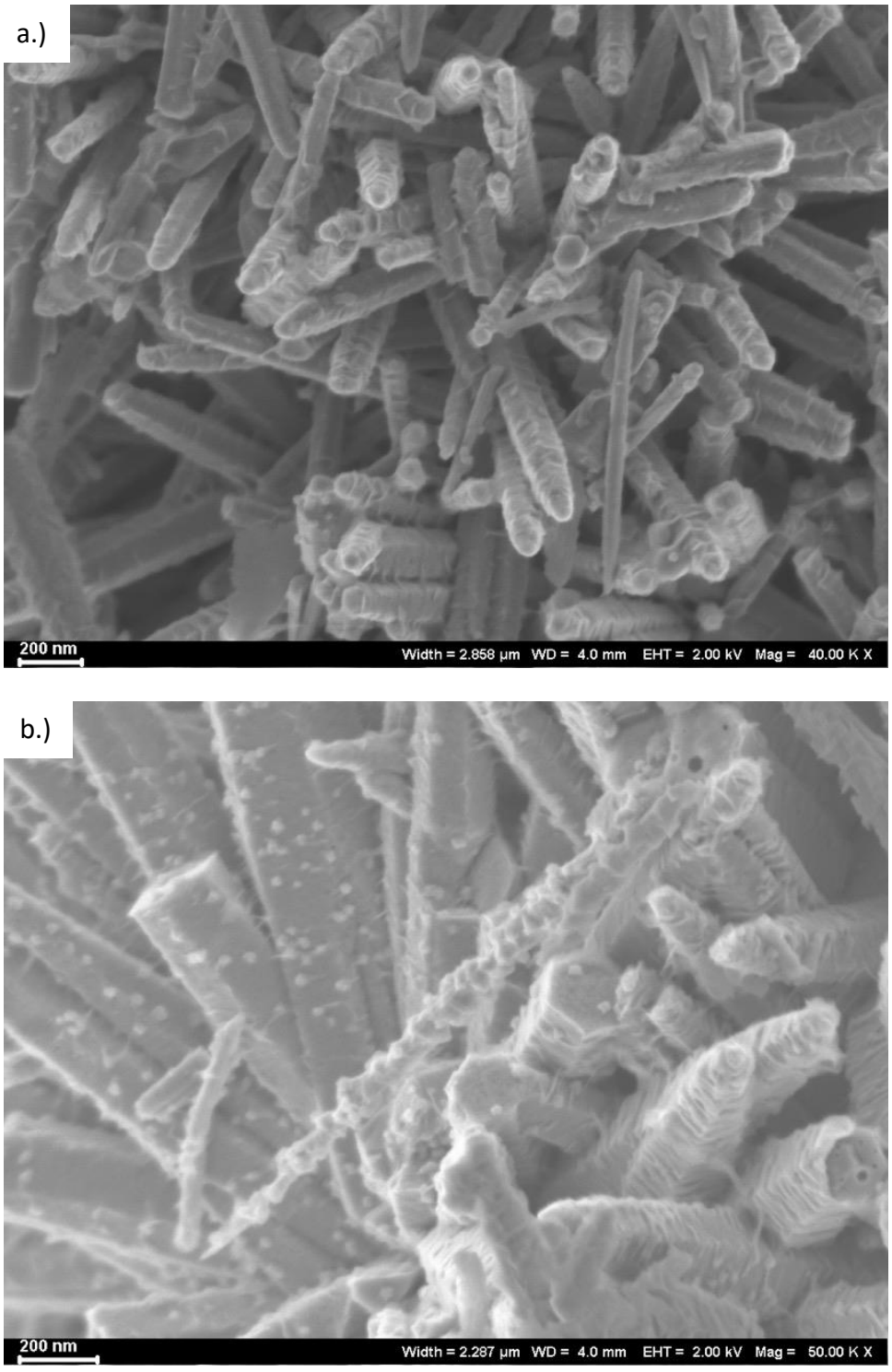

Figure 5.18. SEM of ZnO:CoO Nanorods. a.) CoO films forming orthogonal to the rods c-axis; b.) CoO particles forming on the surface.

The TEM image shown in Figure 5.19 shows a typical ZnO nanorod that is formed from the synthesis. Lattice lines are clearly visible with a lattice spacing of 0.27 nm and matches literature. It is clear that the nanorods are not perfect as there is oxide formation on the surface. This is unavoidable to an extent since the synthesis is not under inert atmosphere and DI water is present in the synthesis.

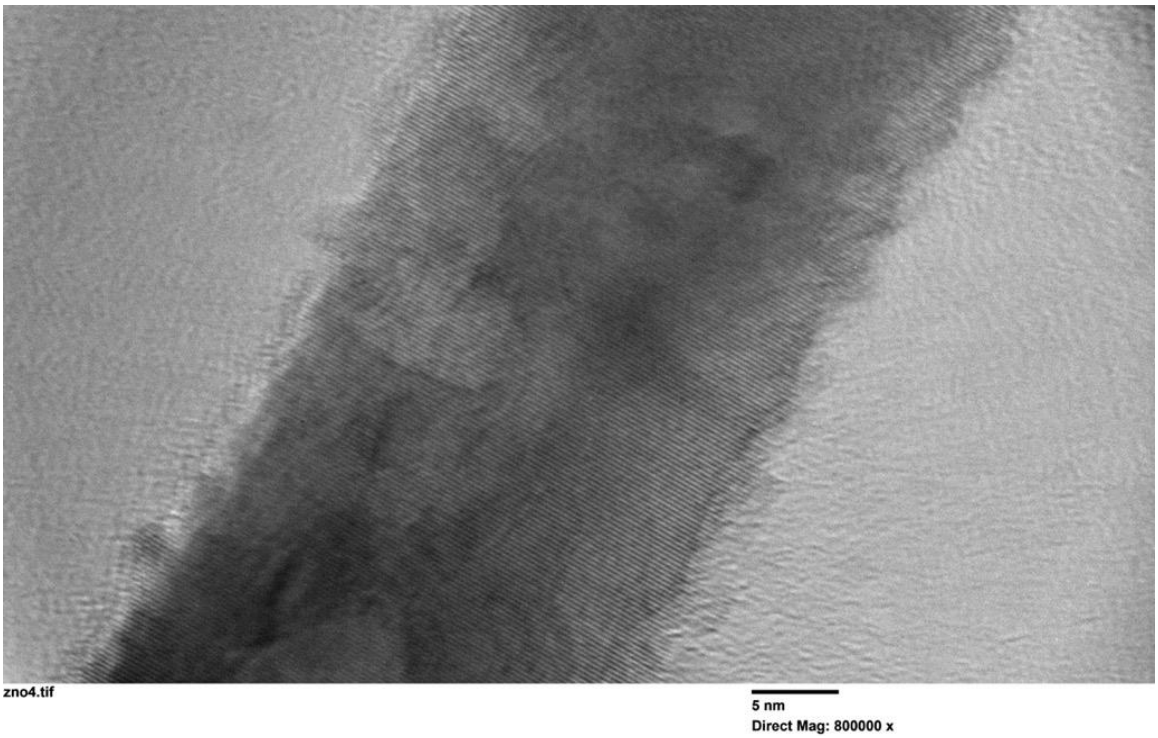

Figure 5.19. TEM Image of Zinc Oxide Nanorod with Lattice Line Resolution.

Figure 5.20a shows a ZnO:CoO NR that is covered in a film but also has nanoparticles on the surface. In Figure 5.20b the micrograph shows the formation of the particles on the surface with lattice line resolution that shows a spacing of .425 nm, which matches literature for the lattice spacing for CoO.

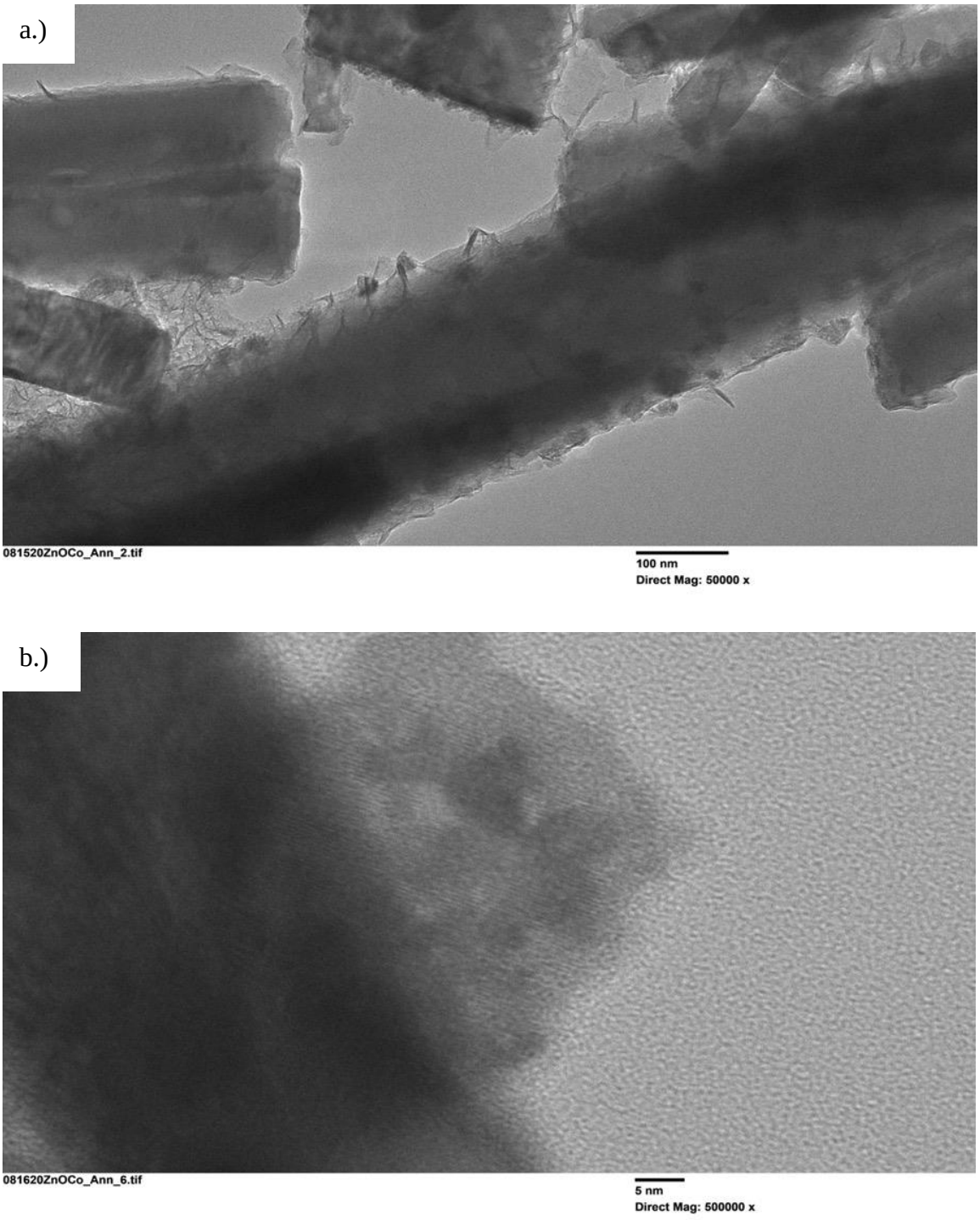

Figure 5.20. TEM Images of ZnO:CoO. a.) ZnO:CoO System Lattice of Zinc Oxide; b.) ZnO:CoO System Lattice of the Cobalt Oxide Particle on the Surface.

To further confirm that the particles are cobalt(II)oxide, STEM/EDS was performed. Figure 5.21a shows a STEM image of the ZnO:CoO system with Figure 5.21b,c giving the mapping of zinc and oxygen that is consistent with Figure 5.21a. In Figure 5.21d, localized concentrations of cobalt are seen on and at the edge of the surface of the ZnO nanorod confirming that the particles have the spectra from XPS, lattice spacing, and elemental analysis showing that they are cobalt(II)oxide particles on the surface of the zinc oxide nanorod. The atomic percentages show zinc at 50.4%, oxygen at 48.5%, and cobalt at 1.1%. This is in good agreement with the other results since the cobalt crystal could not be detected with XRD due to resolution limits.

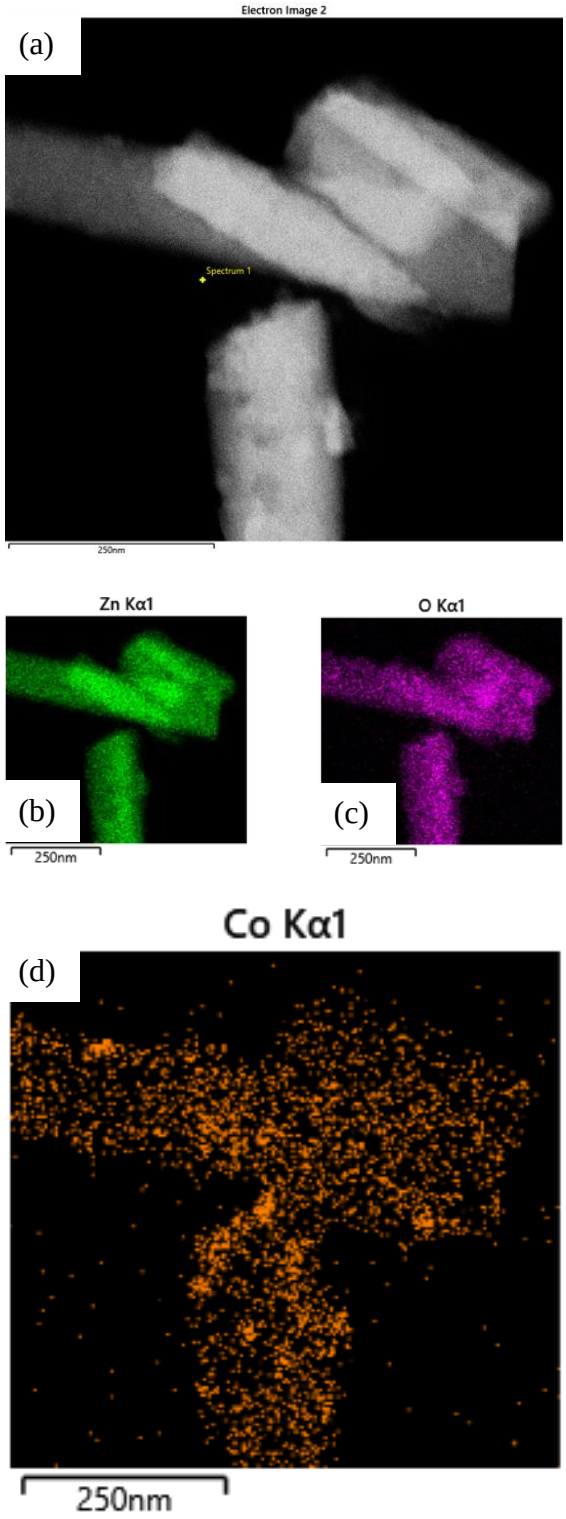

Figure 5.21. STEM/EDS of ZnO:CoO Nanorods.

5.4 References

(1) Ghosh, P.; Sharma, A. K. On-Axis and off-Axis Growth of Zinc Oxide Nanostructures via Pulsed Laser Deposition. *Phys. Status Solidi Appl. Mater. Sci.* **2017**, *214* (5).

(2) Minegishi, K.; Koiwai, Y.; Kikuchi, Y.; Yano, K.; Kasuga, M.; Shimizu, A. Growth of P-Type Zinc Oxide Films by Chemical Vapor Deposition. *Japanese J. Appl. Physics, Part 2 Lett.* **1997**, *36* (11 PART A).

(3) Kato, H.; Sano, M.; Miyamoto, K.; Yao, T. Homoepitaxial Growth of High-Quality Zn-Polar ZnO Films by Plasma-Assisted Molecular Beam Epitaxy. *Japanese J. Appl. Physics, Part 2 Lett.* **2003**, *42* (8 B), 1002–1005.

(4) Saloga, P. E. J.; Thünemann, A. F. Microwave-Assisted Synthesis of Ultrasmall Zinc Oxide Nanoparticles. *Langmuir* **2019**, *35* (38), 12469–12482.

(5) Banerjee, P.; Chakrabarti, S.; Maitra, S.; Dutta, B. K. Zinc Oxide Nano-Particles - Sonochemical Synthesis, Characterization and Application for Photo-Remediation of Heavy Metal. *Ultrason. Sonochem.* **2012**, *19* (1), 85–93.

(6) Ghosh, S.; Majumder, D.; Sen, A.; Roy, S. Facile Sonochemical Synthesis of Zinc Oxide Nanoflakes at Room Temperature. *Mater. Lett.* **2014**, *130*, 215–217.

(7) Garces, H. F.; Espinal, A. E.; Suib, S. L. Tunable Shape Microwave Synthesis of Zinc Oxide Nanospheres and Their Desulfurization Performance Compared with

Nanorods and Platelet-like Morphologies for the Removal of Hydrogen Sulfide. *J. Phys. Chem. C* **2012**, *116* (15), 8465–8474.

(8) Ul Hassan Sarwar Rana, A.; Kang, M.; Kim, H. S. Microwave-Assisted Facile and Ultrafast Growth of ZnO Nanostructures and Proposition of Alternative Microwave-Assisted Methods to Address Growth Stoppage. *Sci. Rep.* **2016**, *6* (April), 1–13.

(9) Šarić, A.; Štefanić, G.; Dražić, G.; Gotić, M. Solvothermal Synthesis of Zinc Oxide Microspheres. *J. Alloys Compd.* **2015**, *652*, 91–99.

(10) Hu, Z.; Oskam, G.; Searson, P. C. Influence of Solvent on the Growth of ZnO Nanoparticles. *J. Colloid Interface Sci.* **2003**, *263* (2), 454–460.

(11) Davis, K.; Yarbrough, R.; Froeschle, M.; White, J.; Rathnayake, H. Band Gap Engineered Zinc Oxide Nanostructures: Via a Sol-Gel Synthesis of Solvent Driven Shape-Controlled Crystal Growth. *RSC Adv.* **2019**, *9* (26), 14638–14648.

(12) Zhao, H.; Rosei, F. Colloidal Quantum Dots for Solar Technologies. *Chem* **2017**, *3* (2), 229–258.

(13) Zhong, X.; Xie, R.; Zhang, Y.; Basché, T.; Knoll, W. High-Quality Violet- To Red-Emitting ZnSe/CdSe Core/Shell Nanocrystals. *Chem. Mater.* **2005**, *17* (16), 4038–4042.

CHAPTER VI

CONCLUSIONS AND FUTURE WORK

6.1 Conclusions

The overall goal for this research described in this dissertation was to take a known material and manipulate the morphology using novel multiple pathways.

There has been a lack of literature involving organic solvents as a means to **Aim 1** of this work was to explore the use of organic solvents and how they impact zinc oxides synthesis. It was seen that different bandgaps can be achieved by varying the solvent in the same synthetic setup. The phenomena can be attributed to how the organic solvents interacted with the zinc oxide sols to form diverse nanostructures due to oriented attachment of the crystal facets during growth. Further morphology characterization with TEM nanorods and that the crystallinity are in good agreement with what was expected. Hydroquinone and DMSO and their respective structures were a collection on sols and or particles that did not have a preferred oriented growth due to those solvents which was further shown by SAED. XRD finalized that the nanostructures were wurtzite hexagonal crystallinity with the exception of DMSO which is believed to be from DMSO with NaOH to form a superbase that does not allow growth to occur. XPS analysis were performed on the sols before solvent was added to the system, m-Xylene, and

hydroquinone. Results showed that there were differences in binding energy for m-Xylene and hydroquinone showing that solvent does affect the crystal packing which was further indicated by XRD. The sols had a most definite difference to the nanostructures showing zinc hydroxide groups and metal hydroxides in the oxygen scans with carbon used as a metric for charge drift.

I-V measurements were performed on 4 systems which were ZnO sols, ZnO hydroquinone, ZnO DMF, and ZnO thin film. It was to be expected that the ZnO sols would perform the worst due to hydroxide groups being insulators and that the thin film would provide the greatest conductivity due to uniformity and lack of defects and/or holes. The DMF ZnO rods performed better than the HQ which is a little surprising seeing how the packing of the HQ would have been far better than the DMF rods. However, the fact that the DMF system were nanorods shows that the preferred growth path makes a difference in conductivity. Therefore, for future ventures it would be advisable to use zinc nanorods mixed with a polymer matrix if photovoltaics is pursued.

Aim 2 further developed the novel solvent-based synthetic pathway and incorporated dopant materials into the system. Optical bandgap was checked to see if the dopants had any effect. All dopants in the system exhibited a slight red shift all within 2 nm of each other who's dopant levels ranged from 0.5% - 5%. One thing to note is that certain dopants did broaden the ZnO peak significantly which would allow better absorption of light for a photovoltaic while other maintained its sharp assent like the unmodified ZnO.

X-ray diffraction was done to check if dopants had been incorporated into the lattice by observing a shift in any of the three main peaks of the wurtzite structure. Shifts did occur in all dopants but the three largest shifts were copper, cobalt, and erbium respectively. Chromium and iron gave minimal shift and their pattern register other peaks along with the wurtzite structure which is a heavy indicator for side reaction material to be formed.

SEM was done to see if the synthesis enabled the morphology to maintain as hexagonal rods of similar dimensions. Only copper and erbium maintained singular morphology in the system being nanorods. All other dopants either did not form nanorods or had mixed morphologies. This is probably due to how fast the hydrolysis step is consumed. More specifically, the zinc sol and residual dopant ions compete for the sodium hydroxide which causes the morphology to be non-homogeneous. If this were to be done again, metal precursors would be mixed thoroughly before the inclusion of sodium hydroxide, then after more stirring, DMF would be added. One thing to note is that Copper in higher dopant concentrations was able to facilitate hierarchical structures with the zinc oxide. This could lead to new pathways for reactions that involve safe, low temperature environments that otherwise might require high temperatures and/or dangerous procedures.

Aim 3 was to verify if post modification could be achieved using only precursor material and aqueous conditions to obtain a core/shell system with cobalt. XRD was done to show that the amount of cobalt in the system could not be detected by this technique to verify the crystal structure of what cobalt was forming into. SEM and TEM analysis was

done and showed that at a certain temperature, a cobalt oxide film would form into cobalt oxide particles. The lattice spacing for the cobalt oxide particles was 0.425 nm which is in good agreement with literature for Co^{2+} state. The oxidation state of cobalt was further verified using XPS. Specifically, by the use of satellite peaks and their binding energy rather than cobalt and its 2p orbital split. This concludes that particle formation on the surface is in fact CoO where this is probably due to localized nucleation on the ZnO rod formed from defects on the surface. Hence why particles are formed and not a shell. From our understanding, this is the first report of cobalt oxide particles have been formed on the surface of another nanostructure.

6.2 Future Work

This dissertation has let to interesting phenomena that can lead to future research to be pursued. In this chapter, a discussion of opportunities that can be taken over by fresh, optimistic students.

6.2.1 Solvent Study

There are promising avenues when modifying the synthesis of zinc oxide with solvents. A possible alternative would to use the modified Hansen solubility parameters. These parameters make note of solvents and certain properties and then by mixing different solvents together they achieve the same effect as an expensive solvent. This technique is primarily used in the polymer industry but could be applied to nanoparticle systems to control the morphology of zinc oxide or any metal oxide synthesis.

6.2.2 Doping Study

Literature and this dissertation have shown doping is possible and that morphology can be somewhat controlled. More importantly, morphology control based on dopant could be a plausible avenue for future research as well as involving different solvents to fine tune the process.

6.2.3 Core/Shell Study

Future directions for this study can take two paths. The first is using alternative solvents as a means to affect how the cobalt is grown on the surface of the rod. Another path would be to apply this same method but use other first row transition metals and see if nanoparticle growth is possible for those metals or if there is another metal that could be a better core/shell system with this method. The third would to be combine the two ideas and see if different solvents with a variety of different first row metals can produce the same or better results described in this dissertation.